View Online / Journal Homepage / Table of Contents for this issue
Dynamic Article Links

Organic & Biomolecular Chemistry

Cite this: *Org. Biomol. Chem.*, 2012, **10**, 7402

www.rsc.org/obc

PAPER

Development of a novel class of B-Raf^{V600E}-selective inhibitors through virtual screening and hierarchical hit optimization†

Xiangqian Kong,‡[a] Jie Qin,‡[b] Zeng Li,‡[a] Adina Vultur,[b] Linjiang Tong,[a] Enguang Feng,[a] Geena Rajan,[b] Shien Liu,[a] Junyan Lu,[a] Zhongjie Liang,[a] Mingyue Zheng,[a] Weiliang Zhu,[a] Hualiang Jiang,[a] Meenhard Herlyn,[b] Hong Liu,*[a] Ronen Marmorstein*[b] and Cheng Luo*[a,c]

Received 5th June 2012, Accepted 10th July 2012
DOI: 10.1039/c2ob26081f

Published on 13 July 2012 on http://pubs.rsc.org | doi:10.1039/C2OB26081F
Downloaded by University of California - San Diego on 01 September 2012

Oncogenic mutations in critical nodes of cellular signaling pathways have been associated with tumorigenesis and progression. The B-Raf protein kinase, a key hub in the canonical MAPK signaling cascade, is mutated in a broad range of human cancers and especially in malignant melanoma. The most prevalent B-Raf^{V600E} mutant exhibits elevated kinase activity and results in constitutive activation of the MAPK pathway, thus making it a promising drug target for cancer therapy. Herein, we describe the development of novel B-Raf^{V600E} selective inhibitors *via* multi-step virtual screening and hierarchical hit optimization. Nine hit compounds with low micromolar IC_{50} values were identified as B-Raf^{V600E} inhibitors through virtual screening. Subsequent scaffold-based analogue searching and medicinal chemistry efforts significantly improved both the inhibitor potency and oncogene selectivity. In particular, compounds **22f** and **22q** possess nanomolar IC_{50} values with selectivity for B-Raf^{V600E} *in vitro* and exclusive cytotoxicity against B-Raf^{V600E} harboring cancer cells.

Introduction

The evolutionarily conserved Ras/Raf/MEK/ERK mitogen-activated protein kinase (MAPK) signaling pathway, relaying the proliferative signals generated by cell surface receptors and cytoplasmic signaling components into the nucleus, is a critical regulator of many cellular processes involved in cell proliferation, differentiation, and survival.[1–3] Aberrant activation of the MAPK pathway represents a common indicator for a wide variety of proliferative diseases and especially cancer.[4,5] Moreover, accumulating data demonstrates that high-frequency activating mutation[6–8] or amplification[9–11] at several levels in this pathway greatly prompts multiple tumor oncogenic processes, such as cell immortalization, angiogenesis, invasive growth, metastases and drug resistance.[12–14] Therefore, the Ras/Raf/MEK/ERK signaling cascade has become one of the primary candidates for novel molecular targeted cancer therapies.[15–17]

The Raf serine/threonine kinase family was initially identified as a cellular homolog of the retroviral oncogene v-Raf and consists of three isoforms named Raf-1 (C-Raf), A-Raf and B-Raf.[18–20] Distinct from other Raf paralogs, B-Raf requires fewer post-translational modifications for optimal activation and possesses substantially greater basal activity.[21,22] In addition, B-Raf has also been shown to be the major Raf effector in the MAPK signaling cascade.[23–26] All of these unique properties in cellular physiology provide a molecular shortcut for B-Raf activation and greatly substantiate the potential of B-Raf to be a *bona fide* oncogene.[27] The importance of B-Raf in oncogenesis is highlighted by the finding that it is mutated in approximately 7% of human cancers, with the highest incidence in malignant melanoma (60%–70%), thyroid (30%–50%), ovarian (~30%) and colorectal (5%–20%) carcinomas, and with a relatively lower frequency (1%–3%) in a wide variety of other cancers.[7,28] Among more than 75 identified B-Raf mutations in human cancers, a Glu for Val substitution at residue 600 in the kinase domain accounts for over 90% of B-Raf mutations, which harbors 500-fold higher intrinsic kinase activity.[29] The B-Raf^{V600E} could effectively circumvent the requirement of phosphorylation-dependent regulation by Ras, and result in constitutive activation of the MAPK signaling pathway, even in the absence of extracellular mitogenic stimuli, facilitating the malignant transformation.[30,31] The presence of B-Raf^{V600E} in certain

[a]*State Key Laboratory of Drug Research, Shanghai Institute of Materia Medica, Chinese Academy of Sciences, Shanghai 201203, China. E-mail: cluo@mail.shcnc.ac.cn, hliu@mail.shcnc.ac.cn; Fax: +86-21-50807088; Tel: +86-21-50271399*
[b]*The Wistar Institute, Philadelphia, PA 19104, USA. E-mail: marmor@wistar.org; Fax: +0-215-898-0381; Tel: +0-215-898-5006*
[c]*Center for Systems Biology, Soochow University, Jiangsu 215006, China*

†Electronic supplementary information (ESI) available. See DOI: 10.1039/c2ob26081f

‡These authors contributed equally to this work.

This journal is © The Royal Society of Chemistry 2012

Published on 13 July 2012 on http://pubs.rsc.org | doi:10.1039/C2OB26081F
Downloaded by University of California - San Diego on 01 September 2012

cancer cohorts also correlates with the increased risk of deterioration and poor prognosis.[32,33] Taken together, these findings strongly suggested that B-Raf is a promising therapeutic target in melanoma and other carcinomas that depend upon B-Raf signaling.

Given the significance of B-Raf in tumorigenesis and progression, the inhibitors targeting B-Raf and especially the oncogenic forms of B-Raf, have increasingly come into the limelight of the drug discovery arena. To date, a number of oncogenic B-Raf inhibitors have been reported in various developmental stages.[34–39] Some of them have entered clinical trials in recent years and exhibit encouraging clinical efficiency.[40–42] Among them, Vemurafenib, which was approved by the FDA and EMA (European Medicines Agency) for the treatment of unresectable or metastatic melanoma, is characterized as a selective B-Raf^{V600E} inhibitor.[43] It demonstrated complete or partial tumor regression in the majority of patients harboring the B-Raf^{V600E} mutation and with an overall increased median survival time after the treatment, which validates the effectiveness of targeting the oncogenic B-Raf in cancer therapy.[40,44] However, the emerging data also indicates that some mutant B-Raf tumors have intrinsic resistances to B-Raf inhibitors accessed clinically to date, and the acquired resistance occurred through a variety of mechanisms.[45–47] Furthermore, a series of side effects have also been observed, in particular the induction of keratoacanthoma was frequently observed in Vemurafenib treated patients.[44] Therefore, there is clearly an unmet therapeutic need to develop novel, potent and specific B-Raf inhibitors possessing different properties to benefits the patients with B-Raf^{V600E}-driven cancers.

Structure based virtual screening (SBVS) has become a powerful tool in the medicinal chemists' toolkit, and the incorporation of the characteristic information from the known active ligands into the virtual screening campaign could further improve the hit enrichment as well as the potential for scaffold hopping.[48,49] In the present study, a combined ligand- and structure-based virtual screening protocol was employed to discover novel B-Raf^{V600E} inhibitors. Nine structurally novel hit compounds with high ligand efficiency were successfully identified. Subsequent scaffold-based analogue searching and structure optimization significantly increased the inhibitory potency and B-Raf^{V600E} selectivity in both enzymatic and cellular assays. In particular, compound **22q** possesses excellent *in vitro* and *ex vivo* B-Raf^{V600E} inhibitory potency and exhibits cellular selectivity towards B-Raf^{V600E} harboring cancer cell lines.

Results and discussion

Virtual screening

To strengthen the efficiency of scaffold hopping and hit discovery rate, we designed an integrated ligand- and structure-based virtual screening procedure aimed to counterbalance their fundamental limitations.[49] The SHAFTS algorithm, which is a hybrid 3D molecular similarity calculation approach designed to combine the strength of pharmacophore matching and volumetric overlay, exhibiting satisfactory "scaffold hopping" capability against several representative kinases,[50–52] was utilized for ligand-based virtual screening (LBVS). Since the shape and volume of the ATP binding pockets are altered upon different ligand binding, two crystal structures of B-Raf in the active conformation (PDB entry: 3og7,[40] 2fb8[35]) varied in binding pocket architecture were used for conducting the structure-based virtual screening with the GLIDE program,[53] which achieved the best performance in our pilot study (see ESI† for detailed results). A schematic representation of the overall virtual screening procedure in this study is presented in Fig. 1. Taking the respective bioactive conformations of Vemurafenib (Template 1) and SB-590885 (Template 2) in complex with B-Raf as queries,[35,40] SHAFTS was utilized to search the SPECS vendor databases which contains more than 200 000 compounds. The top 1000 molecules with similarity scores >1.0 were reserved for each template, which resulted in 581 hits for template 1 and 1000 hits for template 2. These compounds were then docked into their corresponding structures with GLIDE using the standard precision (SP) mode, and the top 500 compounds for each structure were submitted for further docking validation using the GLIDE extra precision (XP) mode and visual inspection. The candidate molecules were selected based on the following criteria: (1) The molecular weight of the ligand was lower than 500 Da, rendering it suitable for further optimization. (2) Both geometric and chemical features matching existed between the ligand and the ATP binding site of B-Raf. (3) The binding poses and chemical structures were reasonable. Some highly ranked molecules that displayed either high strain energy or excessive rotatable bonds were rejected from further evaluation. (4) At least one H-bond was formed by the ligand with the backbone atoms of the hinge region residues (such as Q530 and C532), which are critical for anchoring the inhibitors in the active site.[54] (5) The hydrophobic pocket surrounding the gatekeeper residue (back pocket) was occupied by the corresponding lipophilic groups in the ligand, which plays important roles in determining both the kinase selectivity and inhibitor binding affinity.[55,56](6) The ligands were prioritized for selection if at least one H-bond interaction was formed with the "DFG-motif" of B-Raf, based on the presumption that it may stabilize the active conformation and improve oncogenic B-Raf selectivity.[38,40] Consequently, 327 compounds that met the above criteria were selected for further scaffold diversity analysis with the Cluster Molecules component in Pipeline Pilot 7.5. One or two candidate molecules with relatively simple chemical structure and higher GLIDE score (G-score) within each structural cluster were retained. Finally,

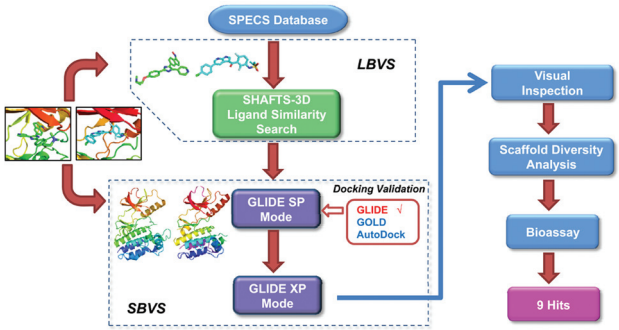

Fig. 1 Schematic representation of the virtual screening strategy adopted in the present study.

Published on 13 July 2012 on http://pubs.rsc.org | doi:10.1039/C2OB26081F
Downloaded by University of California - San Diego on 01 September 2012

Table 1 Inhibition rates (%) or IC_{50} values against B-Raf^{V600E} of the hits derived from virtual screening

Compound	IC_{50} (μM) or inhibition rate[a] (%)
1	3.189 (3.238)[b]
2	79%
3	52%
4	60%
5	3.984 (3.699)[b]
6	53%
7	86%
8	50%
9	67%

[a] Inhibition rate at 5 μM of compound. [b] The IC_{50} values for both B-Raf^{V600E} and wild-type B-Raf (in the parentheses) were determined for the 2 most potent compounds against B-Raf^{V600E}.

113 compounds were designated for purchase for B-Raf inhibition activity assessment.

In vitro inhibition assay against B-Raf^{WT} and B-Raf^{V600E} kinases

The 113 candidate molecules selected by virtual screening were tested for B-Raf^{WT} and B-Raf^{V600E} inhibition as previously described.[36,39] Nine compounds with diverse chemotypes demonstrated significant inhibition for B-Raf^{V600E} activity at 5 μM in the preliminary test, and the IC_{50} values towards both B-Raf^{WT} and B-Raf^{V600E} were then determined for the two most potent hit molecules (Table 1). Among the two hits possessing low-micromolar IC_{50} values against both wild-type and B-Raf^{V600E}, compound **1** was characterized as a structurally novel B-Raf inhibitor with higher ligand efficiency (0.42 kcal mol^{-1} per heavy atom *versus* 0.24 kcal mol^{-1} per heavy atom of hit **5**)[57] in inhibiting B-Raf^{WT} and B-Raf^{V600E} activity. Moreover, compound **1** also exhibited encouraging anti-proliferation activity. It could efficiently inhibit the proliferation of both A375 (B-Raf^{V600E} mutant) metastatic melanoma and HCT-116 (Ras mutant) colon carcinoma cells at 10 μM in which the hyperactivated MAPK pathway was the main molecular driver for tumorigenesis (Table S4†), implicating that the cytotoxicity of hit **1** may be attributed to its *in vivo* MAPK pathway inhibition. It is also noteworthy that the B-Raf^{V600E} harboring A375 melanoma cells were more sensitive to hit **1** than HCT-116 cancer cells that contain B-Raf^{WT}. Taken together, these data suggested that hit **1** represented a novel B-Raf^{V600E} selective chemotype with high ligand efficiency and promising anti-proliferation activity, offering a good starting point for further optimization.

Scaffold-based analogue searching

Upon close examination of the binding mode of compound **1** (Fig. S2†), we noted that the nitro group attached to the exocyclic methylene could form a hydrogen bond with the amide nitrogen of Cys532 in the hinge area, and the 5-phenylfuran moiety exhibited significant shape complementation with the ATP-binding site to make extensive hydrophobic interactions with the back pocket around the gatekeeper residue. On account of the fact that the nitro group generally functioned as a relatively weak H-bond acceptor in molecular interactions and has a relatively small VDW volume,[58] we then assumed that a novel hinge region binder with more favorable H-bond and VDW interacting capability may improve both the inhibitory potency and oncogenic B-Raf selectivity. Therefore, a substructure-based analogue searching with 2-phenyl-5-vinylfuran (highlighted in red in Fig. 2) as a query template was performed to hop the potential hinge region binders, and a focused library comprising of all of the hit compounds was extracted from the SPECS database. Then the focused library was docked into the active site of B-Raf with GLIDE program and ranked by G-score. After visual inspection, nineteen compounds with the same scaffold but with diverse substitutions on the exocyclic methylene and phenyl were purchased from the vendor database and their inhibitory activities against both B-Raf^{WT} and B-Raf^{V600E} were assessed. As shown in Table 2, 12 out of 19 compounds exhibited more than 50% inhibition of B-Raf^{V600E} activity at 5 μM. Apparently, independent of the distinct substitutes on the exocyclic methylene, smaller hydrophobic substitutes (*e.g.* halogen in compound **17–19**, **24**) could be well tolerated in the *para* position of the phenyl group, and kinase inhibitory activity was completely abolished in the case of *ortho*- and *para*-double substitution (*e.g.* **15**, **20**, **21**). However, the broad activity spectrum for both the *ortho*- and *meta*-substituted compounds indicated that the potency and selectivity against B-Raf^{V600E} were remarkably affected by the different furan-2-methylene substitutes (*e.g.* compound **11** and **26**, or compound **12**, **23** and **27**), which was consistent with our assumption and underlined the importance of selecting proper hinge binders for further optimization. It is also notable that most of the inhibitors showed varying degrees of selectivity against B-Raf^{V600E} over B-Raf^{WT}, especially for compounds **11**, **19** and **22**, which showed about 2–3 fold selectivity. In summary, although no significant improvement in inhibitory potency was observed for these analogues over the original hit, they did provide novel chemotypes with enhanced oncogene selectivity for further evaluation. In view of the biological potency, oncogene selectivity and chemical feasibility, compounds **16**, **17**, **19** and **22**, which contained the 2,3-dihydro-1*H*-inden-1-one, indolin-2-one, thiazolidine-2,4-dione and 2-thiobarbituric acid moieties respectively, were selected for hit optimization and structure–activity relationship (SAR) study.

Hit optimization and SAR analysis

To confirm the effectiveness of the hits identified through the scaffold searching procedure and explore their preliminary structure–activity relationship (SAR), we initiated the hit optimization campaign. According to isosteric replacement theory and synthetic feasibility, the bivalent sulfur atom in the 2,3-dihydro-1*H*-inden-1-one moiety of hit **16** was replaced by a methylene group, for which the activity was confirmed by subsequent experimental evaluation (**16e**). In total, 35 compounds were designed and synthesized, and their chemical structures are shown in Tables 3–5.

The general synthetic route of the designed compounds **16a–g**, **17a–f**, **19a–k** and **22a–q** is depicted in Scheme 1. 5-Formyl-2-furanboronic acid was treated with various

 This journal is © The Royal Society of Chemistry 2012

Published on 13 July 2012 on http://pubs.rsc.org | doi:10.1039/C2OB26081F
Downloaded by University of California - San Diego on 01 September 2012

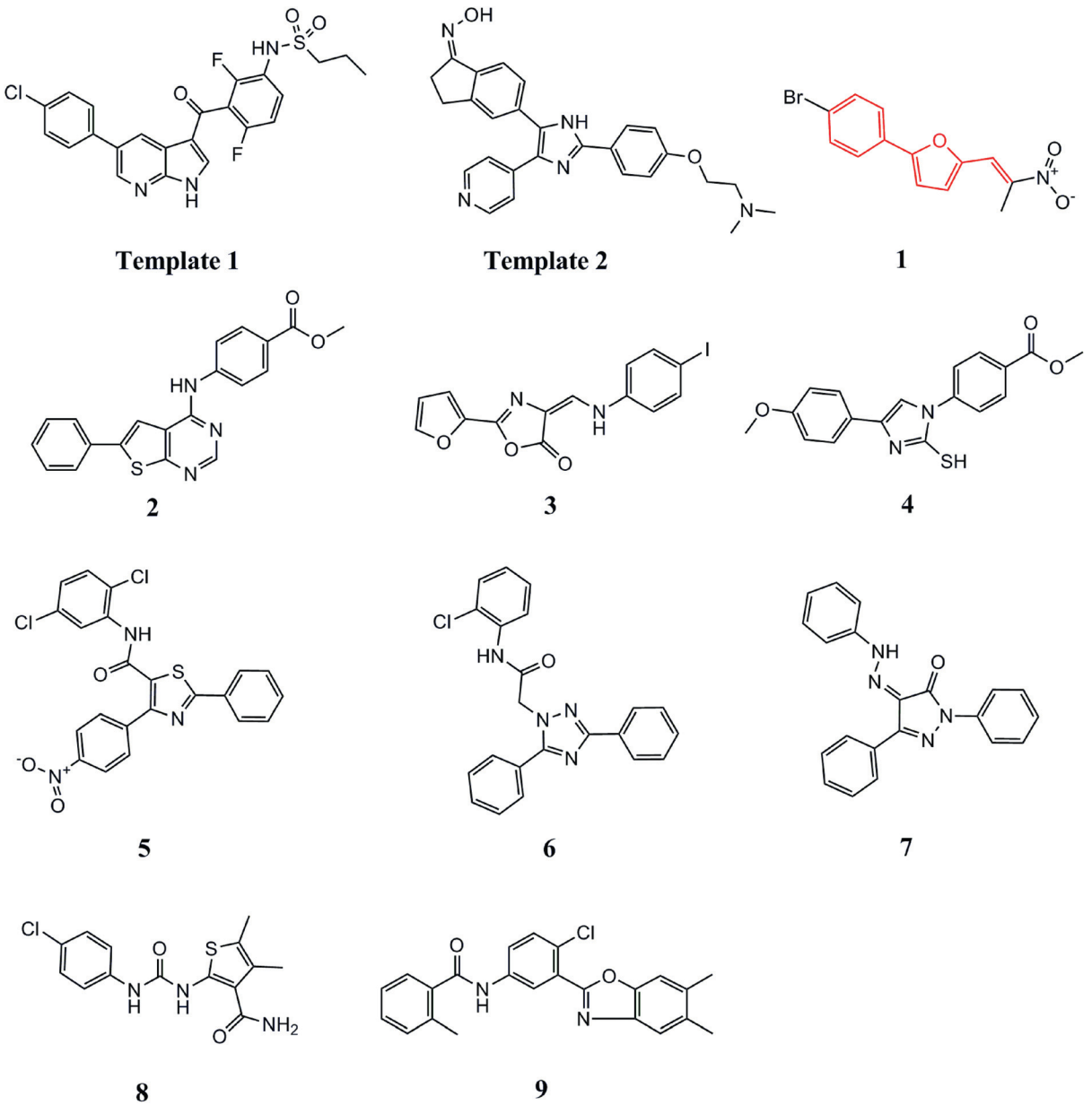

Fig. 2 Chemical structures of the query templates employed in SHAFTS searching and hit compounds identified from virtual screening. The structural moiety of hit **1** used in the substructure search is highlighted in red.

substituted bromobenzenes, $Pd(PPh_3)_4$ and K_2CO_3 to yield compounds **30**. Then the final products (**16a–g**, **17a–f**, **19a–k** and **22a–q**) were obtained using the Knoevenagel condensation between compound **30** and various substituted 1-indanone, 2,3-dihydroindol-2-one, 2,4-thiazolidinedione and 2-thiobarbituric acid, respectively. The crude products were purified by washing with MeOH or recrystallizing from EtOH to yield pure products.

The *in vitro* kinase inhibition assay clearly indicated that distinct substitutes on the exocyclic methylene had a significant effect on both the inhibitory potency and B-Raf^{V600E} selectivity. Of the synthetic derivatives tested, 13 compounds (*e.g.* **16a**, **16c**, **16e**; **22a–c**, **22e–k**) exhibited more than 50% inhibition against B-Raf^{V600E} at 2 μM, wherein most of the compounds were close analogues of hit **22**, which contained a 2-thiobarbituric acid moiety as the potential hinge binder (Tables 3–5). However, on the whole, the majority of the derivatives of hit **16**, **17** and **19** displayed relatively weak inhibition in comparison with that of hit **22**, which was more visible when the same substituents were present on the benzene ring (*e.g.* **22a** *vs.* **16a** and **19a**, **22f** *vs.* **16f** and **19**, **22k** *vs.* **17d** and **19k**). Moreover, while the three analogues of hit **16** (**16a**, **16c**, **16e**) exhibited encouraging inhibitory activity at 2 μM, their activities declined at lower concentration. In contrast, significant inhibitory potency could still be observed for five derivatives of hit **22** at the same concentration (**22f–h**, **22j**, **22k**) and was exemplified by the 2–5 fold improvement in their IC_{50} values compared with the original hit (Table 5). Collectively, the data from the preliminary optimization highlighted the optimal performance of the 2-thiobarbituric acid analogues with respect to B-Raf^{V600E} inhibition.

View Online

Table 2 Structure and potency of the compounds identified from the substructure-searching

ID	Structure	IC_{50}[a] (μM) or inhibition rate[b] (%) B-Raf	B-Raf^{V600E}	ID	Structure	IC_{50}[a] (μM) or inhibition rate[b] (%) B-Raf	B-Raf^{V600E}
1	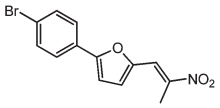	3.24[c]	3.19[c]	**19**	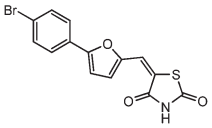	4.99	2.26
10	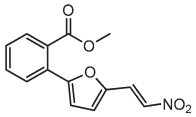	1.38	1.96	**20**	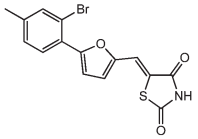	n.a.	n.a.
11	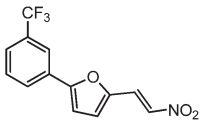	4.04	2.78	**21**	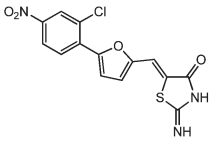	n.a.	n.a.
12	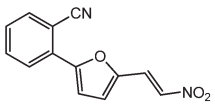	43% 17%	28% 18%	**22**	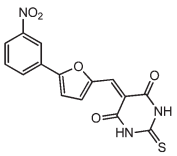	6.60	2.09
13	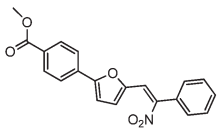	20% n.a.	56% 27%	**23**	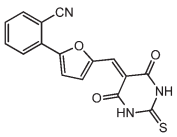	62% 36%	75% 42%
14	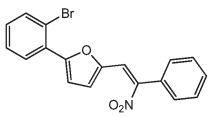	50% 21%	40% 30%	**24**	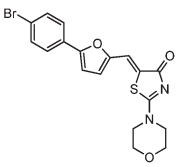	46% n.a.	53% 30%
15	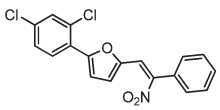	n.a.	n.a.	**25**	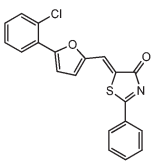	43% 24%	72% 58%
16	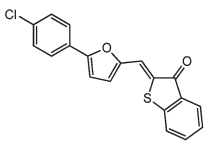	62% 50%	78% 61%	**26**	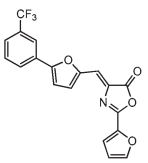	n.a.	n.a.
17	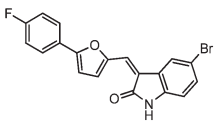	2.98	3.85	**27**	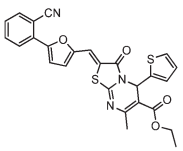	30% 14%	68% 49%
18	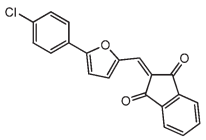	40% 14%	67% 38%	**28**	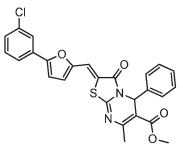	32% 17%	47% 40%

[a] IC_{50} values were determined if the inhibition rate at 2 μM was larger than 65%. [b] For each compound, the values listed in the upper and lower panels of the cell refer to the inhibition rate (%) at 5 μM and 2 μM, respectively. [c] Values listed for comparison. n.a. = not active.

Downloaded by University of California - San Diego on 01 September 2012
Published on 13 July 2012 on http://pubs.rsc.org | doi:10.1039/C2OB26081F

 This journal is © The Royal Society of Chemistry 2012

Published on 13 July 2012 on http://pubs.rsc.org | doi:10.1039/C2OB26081F
Downloaded by University of California - San Diego on 01 September 2012

Table 3 Chemical structures and activities for the analogues of compound **16**

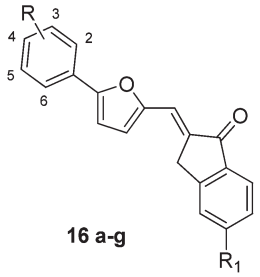

16 a-g

Compound	Substituent R	R1	Inhibition rate[a] (%) B-Raf	B-Raf^{V600E}
16a	2-NO_2	H	11 n.a.	64 47
16b	3-CF_3	H	n.a. n.d.	22 n.d.
16c	3-CF_3	Cl	n.a. n.a.	59 42
16d	4-NO_2	H	n.a. n.d.	34 n.d.
16e	4-Cl	H	n.a. n.a.	52 41
16f	4-Br	H	n.a. n.d.	42 n.d.
16g	2-Cl, 4-CF_3	H	n.a. n.d.	44 n.d.

[a] For each compound, the values listed in the upper and lower panels of the cell refer to the inhibition rate (%) at 2 μM and 0.5 μM, respectively. n.a. = not active. n.d. = not determined.

Table 4 Chemical structures and activities for the analogues of compound **17**

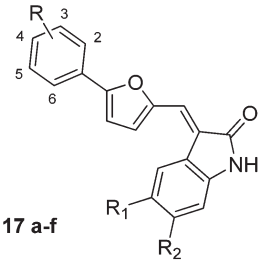

17 a-f

Compound	Substituent R	R1	R2	Inhibition rate[a] (%) B-Raf	B-Raf^{V600E}
17a	3-CF_3	H	H	n.a. n.d.	34 n.d.
17b	3-CF_3	H	Cl	n.a. n.d.	38 n.d.
17c	3-CF_3	Cl	H	17 n.d.	23 n.d.
17d	2-Cl,5-CF_3	H	H	n.a. n.d.	23 n.d.
17e	2-Cl, 5-CF_3	H	Cl	n.a. n.d.	34 n.d.
17f	2-Cl, 5-CF_3	Cl	H	n.a. n.d.	34 n.d.

[a] For each compound, the values listed in the upper and lower panels of the cell refer to the inhibition rate (%) at 2 μM and 0.5 μM, respectively. n.a. = not active. n.d. = not determined.

Analyzing the data in Table 5, we found that either small or bulky hydrophobic substituents, such as methyl, methoxyl, halogens and tertiary butyl retained or improved the inhibition activity to varying degrees (*e.g.* **22e–i**), with the inhibition rate ranging from 30–60% at 0.5 μM, and it was more evident for compound **22f** which produced a potency of nearly 5-fold over compound **22**. However, the activities substantially decreased when introducing the more polar groups (**22c** and **22d**). Accordingly, the activity is highly sensitive to the physicochemical properties rather than the steric size of the substituents at the *para* position, indicating the existence of a relatively bulky hydrophobic cavity. Similarly, a hydrophobic substituent was desirable at the *meta*-position when comparing the activity differences between **22b** and **22**. Moreover, the presence of a cyano group at the *ortho* position of the benzene ring showed reduced activity relative to the nitro substitution, which may be attributed to the insufficient complementarity with the ATP binding site due to its linear configuration. Nevertheless, the B-Raf^{V600E} selectivity for these analogues did not show concomitant improvement as their biological potency. For example, compound **22f** possessed nanomolar activity but exhibited rare discrimination between B-Raf^{V600E} and B-Raf^{WT}. Consequently, we undertook a second round of hit optimization, mainly focusing on increasing B-Raf^{V600E} selectivity, which is deemed to be critical for maximum therapeutic benefit owing to low cytotoxicity toward normal cells. Meanwhile, with the SAR data in hand, most of the efforts were concentrated on exploring the synergistic effects of the substitutions on the benzene ring. As presented in Table 6, the double substitution at *ortho*- and *para*-positions, as well as the *meta*- and *para*-positions did not show the expected "additive" effect, albeit the corresponding mono-substituent could be well accommodated on the benzene ring (*e.g.* **22n** *vs*. **22a** and **22e**, **22p** vs. **22l** and **22e**). Considering the observation that the presence of a H-bond acceptor at the *meta*-position of the benzene improved the B-Raf^{V600E} selectivity, for example with compound **22**, and that the configurational freedom of the methoxyl group may hinder the optimal H-bond formation, we speculated that the introduction of a conformationally constrained H-bond partner with enhanced H-bond forming potential, as well as the relatively hydrophobic nature at both *meta*- and *para*-positions may potentiate the B-Raf^{V600E} selectivity. Encouragingly, compound **22q**, with the 3,4-methylenedioxy substituent on the benzene ring, exhibited the expected improvement in both potency and selectivity. It possessed nanomolar inhibitory activity against B-Raf^{V600E} and about 4-fold selectivity over B-Raf^{WT}, which validated the effectiveness of our speculations and underlined the indispensable contributions of a suitable H-bond acceptor substituent at the *meta*-position for B-Raf^{V600E} selectivity.

To evaluate the effects of B-Raf kinase inhibition on cellular characteristics, the anti-proliferation activity of selected B-Raf inhibitors was investigated. As shown in Table 7, compound **22e**, **22f**, **22g**, **22h**, **22i** and **22q** demonstrated potent growth inhibition activity against the B-Raf^{V600E} harboring

Table 5 Chemical structures and activities for the analogues of compound **19** and **21**

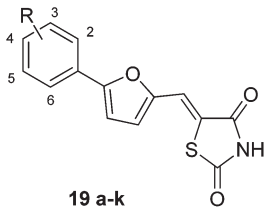

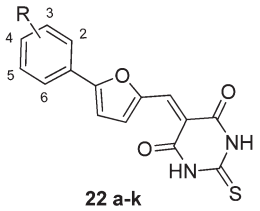

Cmpd.	Substituent	IC$_{50}$[a] or inhibition rate[b] (%) B-Raf	B-Raf^{V600E}	Cmpd.	Substituent	IC$_{50}$[a] or Inhibition rate[b] (%) B-Raf	B-Raf^{V600E}
19a	2-NO_2	n.a. n.d.	7% n.d.	**22a**	2-NO_2	38% n.a.	61% 48%
—	—	—	—	**23**	2-CN	36% 13%	42% 19%
19b	3-OCH_3	n.a. n.d.	34% n.d.	**22b**	3-OCH_3	6% n.a.	63% 34%
—	—	—	—	**22**	3-NO_2	6.60[c]	2.09[c]
19c	4-NO_2	n.a. n.d.	48% n.d.	**22c**	4-NO_2	55% n.a.	59% n.a.
19d	4-CO_2Et	n.a. n.d.	n.a. n.d.	**22d**	4-CO_2Et	n.a. n.d.	38% n.d.
19e	4-Cl	n.a. n.d.	n.a. n.d.	**22e**	4-Cl	15% n.a.	69% 33%
19	4-Br	4.99[c]	2.26[c]	**22f**	4-Br	0.60	0.47
19g	4-Me	n.a. n.d.	41% n.d.	**22g**	4-Me	17% n.a.	59% 50%
19h	4-OCH_3	3% n.d.	41% n.d.	**22h**	4-OCH_3	3.69	2.69
19i	4-tBu	17% n.d.	34% n.d.	**22i**	4-tBu	29% n.a.	57% 36%
19j	Naphthyl	n.a. n.d.	51% n.d.	**22j**	Naphthyl	1.93	1.07
19k	2-Cl,5-CF_3	18% n.d.	37% n.d.	**22k**	2-Cl,5-CF_3	1.49	1.09

[a] IC$_{50}$ values were determined if the inhibition rate at 0.5 μM was larger than 50%. [b] For each compound, the values listed in the upper and lower panels of the cell refer to the inhibition ratio (%) at 2 μM and 0.5 μM, respectively. [c] IC$_{50}$ values were listed for comparison. n.a. = not active. n.d. = not determined.

Downloaded by University of California - San Diego on 01 September 2012
Published on 13 July 2012 on http://pubs.rsc.org | doi:10.1039/C2OB26081F

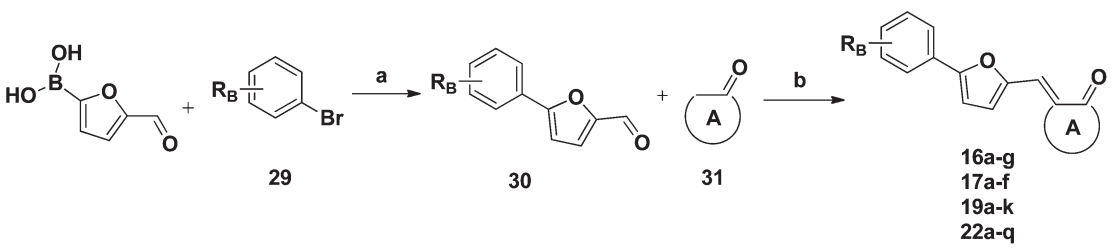

Scheme 1 Reagents and conditions: (a) $Pd(PPh_3)_4$, K_2CO_3, PhMe, 100 °C, 4 h; (b) for the compound **16** series: substituted 1-indanone, NaOH, EtOH, room temperature, 3–4 h; for the compound **17** series: substituted 2,3-dihydroindol-2-one, NaOH, EtOH, room temperature, 3–4 h; for the compound **19** series: 2,4-thiazolidinedione, β-alanine, acetic acid, 90 °C, 2 h; for the compound **22** series: 2-thiobarbituric acid, acetic acid, 90 °C, 2 h.

A375 malignant melanoma cells at 10 μM. Notably, virtually complete growth inhibition for A375 cell lines was achieved by compound **22g**, **22h** and **22i**. On the contrary, anti-proliferation activity toward B-Raf^{WT} containing SW620 human colonic carcinoma cells was observed to modest levels for most of the tested inhibitors, indicating cellular selectivity for B-Raf^{V600E} over B-Raf^{WT} by these compounds. Moreover, the negligible anti-growth activity that was observed for the selected analogues of compound **16** and **19** was consistent with their relatively weak B-Raf^{V600E} inhibitory activity *in vitro* (Table 2), suggesting that the selective targeting of B-Raf^{V600E} was responsible for their cytotoxicity of the analogs of compound **22**.

To further ascertain this selectivity profile, the anti-proliferation effects of compound **22f** and **22q** possessing the most potent B-Raf^{V600E} inhibition potency and selectivity at the enzymatic level were explored in detail against four other human-derived cells. The dose-dependent inhibition profile exemplified in Fig. 3 clearly indicates that B-Raf^{V600E} bearing

 This journal is © The Royal Society of Chemistry 2012

Downloaded by University of California - San Diego on 01 September 2012
Published on 13 July 2012 on http://pubs.rsc.org | doi:10.1039/C2OB26081F

Table 6 Chemical structures and activities for the analogues of **22** in the second round optimization

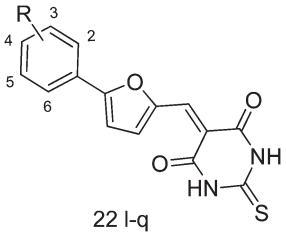

22 l-q

Compound	Substituent	IC_{50}[a] or inhibition rate ([I] = 1 μM) B-Raf	B-Raf^{V600E}
22l	3-CF_3	30%	45%
22m	4-COOH	n.a.	n.a.
22n	2-NO_2, 4-Cl	20%	22%
22o	2-CF_3, 4-Cl	24%	49%
22p	3-CF_3, 4-Cl	37%	48%
22q	3,4-Methylenedioxy	1.15	0.30

[a] IC_{50} values were determined if the inhibition rate at 1 μM was larger than 70%. n.a. = not active.

Table 7 *In vitro* anti-proliferation activity of the selected B-Raf^{V600E} inhibitor at 10 μM

Compound	Tumor growth inhibition rate ([I] = 10 μM) A375(B-Raf^{V600E})	SW620 (B-Raf)
22a	n.a.	n.a.
22b	26.2	n.a.
22c	46.3	n.a.
22e	82.9	9.0
22f	65.3	n.a.
22g	84.0	3.6
22h	94.4	13.0
22i	95.4	7.6
22j	6.9	n.a.
22k	18.3	n.a.
22q	77.7	47.7
19	n.a.	n.a.
16a	16.5	n.a.
16c	3.2	n.a.
16e	5.2	n.a.

n.a. = not active.

tumor cell lines (1205Lu and WM983B) were significantly inhibited following incubation with compounds **22f** or **22q**, whereas normal human primary fibroblasts (FF2508) and malignant cells not expressing mutant B-Raf (WM3918) were significantly more resistant to compound treatment. Notably, the inhibition of tumor growth at 10 μM was more pronounced upon treatment with compound **22q** than compound **22f** (Table 6 and Fig. 3). These results in cells were consistent with the biochemical assays demonstrating that compound **22q** was more potent and selective than compound **22f** against B-Raf^{V600E} (Tables 5 and 6). This correlation between the enzymatic and cellular inhibitory potency again suggested that the anti-growth activity

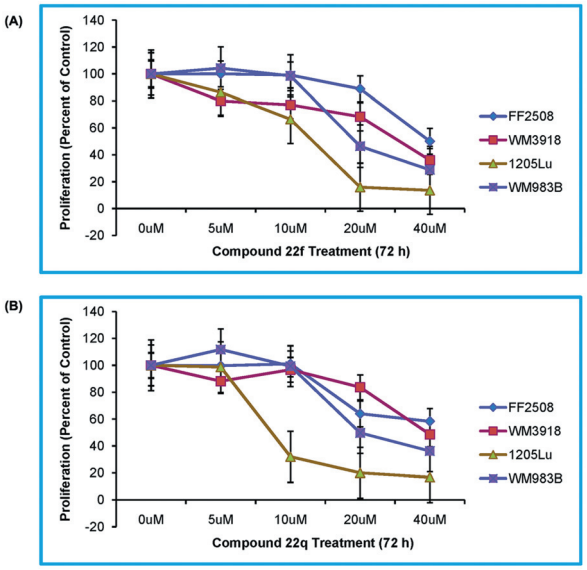

Fig. 3 Effects of the compounds **22f** (A) and **22q** (B) on the proliferation of human-derived cells. Cellular proliferation of melanoma cell lines (WM3918, 1205Lu, WM983B), and human fibroblasts (FF2508) were assessed with the MTS assay. Results are shown as the mean value of four data sets, including standard errors, and are representative of replicated independent experiments. Proliferation is shown as the percent change compared to the vehicle control values.

of the compounds can be well related to their capacity to selectively inhibit oncogenic B-Raf^{V600E} over B-Raf^{WT}. Intriguingly, all of the compounds possessing potent and selective anti-proliferation activity contained the hydrophobic substituent at the *para*-position on the benzene ring, whereas the corresponding polar substitution essentially abolished compound potency. Since the ability of the compounds to penetrate the cell membrane is a prerequisite to cytotoxicity, the *para*-position of the benzene ring may represent a functional site to orchestrate the permeability and cellular activity for 2-thiobarbituric acid B-Raf^{V600E} inhibitors. Taken together, the *ex vivo* anti-proliferation activity data presented here indicates that the biochemical selectivity of the inhibitors (*e.g.* **22q**) against B-Raf^{V600E} translates to the cellular selectivity, reminiscent of the Vemurafenib and SB-590885 compounds that were utilized as the query template during our ligand-based virtual screening and specially targeted the active conformation of B-Raf.

Kinase inhibition profile

To investigate the specificity and selectivity of the identified inhibitors against B-Raf over other kinases, we performed a selectivity profile against a panel of 16 protein kinases at both 5 μM and 1 μM for the two most potent inhibitors **22f** and **22q**. As shown in Table 8, compound **22f** showed only modest levels of inhibition for most of the tested tyrosine- and serine/threonine-kinases except for FGFR1 and IKKβ kinase, which was significantly inhibited at 5 μM. It is noteworthy that the most potent and selective inhibitor **22q**, which was derived from the second round optimization campaign, demonstrated an improved selectivity profile. **22q** significantly inhibited

Downloaded by University of California - San Diego on 01 September 2012
Published on 13 July 2012 on http://pubs.rsc.org | doi:10.1039/C2OB26081F

B-Raf^{V600E} at both concentrations but showed only modest levels of inhibition for these other 16 distinct kinases. Taken together, these data demonstrate that compound **22q** is a B-Raf^{V600E} inhibitor with more than 10-fold selectivity over other tested protein kinases. Collectively, the promising results from this small kinase profiling suggests that compounds **22f** and **22q**, and **22q** in particular, may possess specific inhibitory activity for B-Raf^{V600E}. In addition, these studies also suggest that synergy between *in silico* screening and hierarchical hit optimization can lead to novel B-Raf inhibitors with significant kinase selectivity.

Table 8 Kinase inhibition profile of compound **22f** and **22q** against a panel of 16 protein kinases

	Inhibition rate (%) for compounds at 5 μM and 1 μM			
Kinase	**22f** (5 μM)	**22f** (1 μM)	**22q** (5 μM)	**22q** (1 μM)
SRC	28.3	8.6	15.2	6.2
LCK	10.5	10.5	0.8	n.a.
KDR	6.1	3.9	1.2	n.a.
ABL	n.a.	n.a.	n.a.	n.a.
P38α	7.7	n.a.	n.a.	n.a.
CDK2	39.7	11.6	12.6	3.3
ERK1	30.7	14.5	13.7	10.0
IGF1R	15.6	9.5	6.8	5.6
IKKβ	52.1	27.8	35.7	15.0
PKCα	26.4	16.2	5.2	n.a.
PDGFRα	20.4	7.2	7.7	6.0
EGFR	46.1	12.6	19.4	n.a.
FGFR1	72.2	15.0	18.6	4.9
AKT1	20.3	10.8	14.5	4.6
MET	42.2	34.2	19.4	18.6
cKIT	40.3	18.6	20.0	18.3

n.a. = not active.

Binding mode analysis

To understand the molecular basis for B-Raf^{V600E} inhibition by **22q** and to explore the potential structural origin for the oncogene selectivity, the molecular docking strategy was utilized to scrutinize the binding poses of **22q**. Fig. 4 illustrates the predicted binding poses of **22q** in the ATP-binding site of B-Raf^{V600E} (PDB entry: 3og7[40]). In this model, the 2-thiobarbituric acid moiety is tightly confined within the adenine-binding site of the ATP binding pocket, intercalating between residue W531 and F583 by forming π–π stacking interactions. The amide portion of the 2-thiobarbituric acid group makes bidentate hydrogen bonds with the NH group and the carbonyl oxygen of C532 in the hinge region, forming a "handshake" interaction, which effectively anchors the compound into the ATP binding pocket. The 2-phenyl-5-vinylfuran portion of **22q** extends towards the activation loop (A-loop) and makes extensive hydrophobic interactions with the surrounding residues. In particular, the 3,4-methylenedioxy substituted benzene ring is predicted to occupy the hydrophobic back cavity created by the relatively small gatekeeper residue, mainly comprised of A481, K483, L505, L514, I527, T539 and F595. Gaining access to the kinase back pocket results from the small gatekeeper residue may have the dual effect of not only increasing the biological potency but

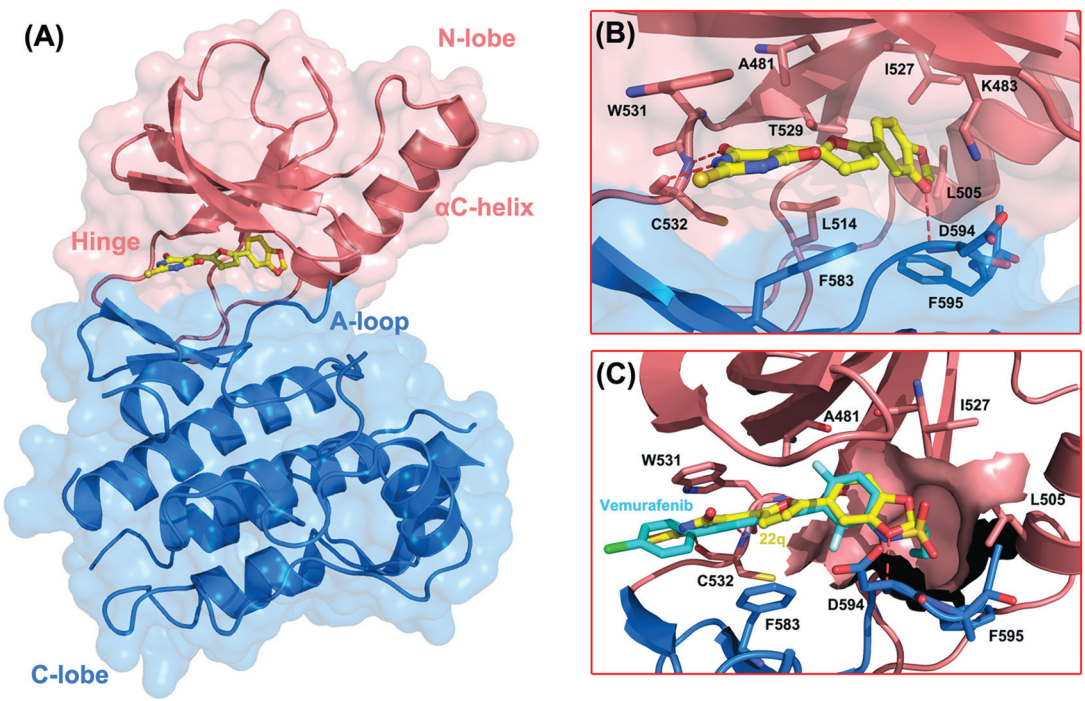

Fig. 4 Binding mode analysis of compound **22q** with B-Raf kinase. (A) B-Raf^{V600E} kinase in the active conformation is shown in cartoon diagram. The N-lobe and C-lobe of B-Raf kinase are shown in pink and blue, respectively. Compound **22q** occupies the ATP binding site between the two lobes represented as yellow sticks. (B) A close-up view of the key interactions between compound **22q** and surrounding residues. Hydrogen bonds are depicted as dotted red lines. (C) Structural comparison of compound **22q** with Vemurafenib (in cyan sticks) in the ATP pocket of B-Raf^{V600E}. The Raf-selective pocket is represented in surface contours.

 This journal is © The Royal Society of Chemistry 2012

Published on 13 July 2012 on http://pubs.rsc.org | doi:10.1039/C2OB26081F
Downloaded by University of California - San Diego on 01 September 2012

also improving the selectivity over other kinases that have a larger gatekeeper residue and hence a smaller back pocket,[56,59,60] which may account for the selectivity profile of **22q**. Notably, the 3,4-methylenedioxy substituent on the benzene ring mediates a hydrogen bond interaction with the backbone NH of D594 in the conserved DFG triad.

The SAR data derived from the two-round structural optimization could be rationalized by the predicted binding mode. The *ortho*-nitro group on the benzene ring may form a weak H-bond interaction with the sidechain of the gatekeeper T529, thus the lower activity that is observed for the linear cyano substitution may partly be attributed to the non-optimal steric complementarity for H-bond formation. Considering the hydrophobic nature of the back cavity, a lipophilic substitution may be preferred over a polar substitution, which was validated by the aforementioned SAR data. In particular, hydrophobic substituents such as methyl, methoxyl and halogens on the *meta*- or *para*-position of the benzene ring (*e.g.* **22f**, **22h**) that would be predicted to better complement the back pocket, achieving elevated shape and chemical feature complementarity with the ATP binding site, greatly contributed to the improved biological potency of the corresponding compounds. Consistent with this notion, the more polar substitutions on the *meta*- or *para*-position of the benzene ring, which would be predicted to be disfavorable due to a high desolvation penalty, showed markedly less potency. For example, nitro, carbethoxy and carboxyl substitutions in these positions showed relatively poor potency (**22c**, **22d** and **22m**). Furthermore, the relatively snug but length-limited back pocket could well accommodate rigid and bulky groups (**22i** and **22j**), however, the more extended substitutions such as carbethoxy group would be predicted to cause some steric clashes when presented at the *para* position of the benzene ring, likely contributing to the weak inhibitory potency of **22d**. It is noteworthy that the presence of a conformationally constrained H-bond acceptor in the *meta*-position of the benzene ring significantly improved B-Raf^{V600E} selectivity (**22**, **22q**). Based on the predicted binding mode, the H-bond acceptor at the *meta*-position of the benzene ring could form a hydrogen bond interaction with the mainchain NH group of D594, reminiscent of a similar interaction observed by Vemurafenib when in complex with B-Raf^{V600E}. The sulfamide moiety in Vemurafenib was deprotonated to facilitate the same hydrogen bond interaction with D564 which was deemed to stabilize the DFG-in conformation and thus contributed to the B-Raf^{V600E} selectivity.[38,40] Moreover, on account of the fact that the conformational equilibrium of B-Raf was strongly biased toward the active state characterized by the DFG-in conformation by the phosphorylation mimic V600E mutation, inhibitors specially targeting the active conformation of B-Raf likely possess higher selectivity against the oncogenic mutant owing to the relatively small configurational entropy cost upon binding.[38–40,43,54,61] In addition, the structural comparison of the active and inactive B-Raf conformation highlights the central role of the mainchain conformation of D594 in directing the conformational switching of the A-loop between the corresponding DFG-in and DFG-out states. Therefore, resembling the important role of the sulfamide in Vemurafenib, the improved selectivity of compound **22** and **22q** for B-Raf^{V600E} over B-Raf^{WT} could be rationalized by the H-bond interaction between the *meta*-substituted hydrogen bond acceptor and the mainchain NH of D594, which potentially stabilizes the DFG-in conformation and the active conformation of B-Raf.

Conclusions and future prospects

Targeted intervention of the *B-Raf*^{V600E} gene product represents a promising approach for cancer therapy. In the present study, we identified a novel class of 2-thiobarbituric acid analogues as selective B-Raf^{V600E} inhibitors by using an integrated ligand- and structure-based virtual screening strategy in conjunction with hierarchical hit optimization. First, the combined ligand- and structural-based virtual screening was utilized for the discovery of structurally novel B-Raf^{V600E} inhibitors. Nine hit compounds with low micromolar activity against B-Raf^{V600E} were successfully identified. Among them, hit **1** was characterized with high ligand efficiency and encouraging anti-proliferation activity, providing an attractive starting point for a hit-to-lead optimization campaign. The molecular modeling study of hit **1** into the ATP-binding site of B-Raf indicated that the biological potency as well as oncogene mutant selectivity could be further optimized by varying the potential hinge region binder and substituent on the benzene ring. The follow-up scaffold-based searching from hit **1** led to a series of B-Raf^{V600E} inhibitors bearing a wide variety of potency and B-Raf^{V600E} oncogene selectivity: four of the analogues of compound **1** displayed potent activities and synthetic feasibility (**16**, **17**, **19** and **22**), so were then selected for hit optimization. Subsequently, the medicinal chemistry effort and SAR analysis was performed to explore the activity and specificity profile of the derivatives for these selected inhibitors, which led to the discovery of 2-thiobarbituric acid analogues with improved inhibitory potency and B-Raf^{V600E} selectivity. The most potent inhibitor, compound **22q**, inhibited the kinase activity of B-Raf^{V600E} with an IC_{50} value in the nanomolar range and with 4-fold selectivity for B-Raf^{V600E} over B-Raf^{WT} and selective cytotoxicity against B-Raf^{V600E} harboring cancer cell lines. In addition, a small kinase profiling study was consistent with the conclusion that the cytotoxicity of the inhibitor was mainly related to the suppression of B-Raf^{V600E} activity.

In addition to providing a novel chemotype with significant biological potency and oncogene selectivity for B-Raf inhibition, the SAR studies and B-Raf^{V600E} selectivity analysis for the 2-thiobarbituric acid analogues offers valuable pharmacophore insights for future optimizations aimed at increasing the inhibitory potency as well as B-Raf^{V600E} mutant selectivity. The structural comparison of **22q** with Vemurafenib in complex with B-Raf^{V600E} reveals that the most significant difference lies in the propyl group in Vemurafenib, which penetrates into the Raf-selective pocket and was proposed to be the critical binding determinant for Raf kinase specificity.[38,40] In the case of compound **22q**, the substitution on the methylene presented in the methylenedioxy group with a short alkyl chain was predicted to occupy this Raf-specific pocket, which potentially augmented the potency and specificity of the inhibitor towards the oncogenic B-Raf^{V600E}. In addition, the structural comparison also reveals that the lipophilic substituent at the *ortho*-position of the benzene ring may further potentiate the hydrophobic interactions with the pocket around the gatekeeper residue. However, it is

Published on 13 July 2012 on http://pubs.rsc.org | doi:10.1039/C2OB26081F
Downloaded by University of California - San Diego on 01 September 2012

noteworthy that the *ortho*-substitution may affect the relative orientation between the benzene ring and the central furan group, which in turn may impede the pivotal hydrogen bond interaction with the beginning of the DFG region. We therefore hypothesize that a relatively small substitution, such as fluorine, chlorine or methyl group may be more desirable at the *ortho*-position. In addition, the NH group in the 2-thiobarbituric acid moiety that does not participate in bidentate hydrogen bonds with the hinge area would be predicted to point towards the solvent. Based on this, we propose that the derivatization at this site such as introducing the solubilizing morpholine fragment may contribute to enhanced solubility and cellular activity.

The study presented here details the optimization process from a fragment-like hit compound derived from virtual screening to a more drug like candidate. This underscores the importance of selecting a proper starting point with low molecular weight and high ligand efficiency to facilitate the subsequent hit-to-lead optimization process. Thus, our study may provide a few useful clues regarding the rational selection of hits for further evaluation. Moreover, the encouraging findings obtained in our study will lay the foundation for future development of more potent and selective oncogenic B-Raf inhibitors for cancer therapy.

Experimental

Computational procedure. Protein preparation

Two representative B-Raf/ligand complexes (PDB entry: 3og7,[40] 2fb8[35]) in the active conformation with apparently distinct shape and volume in the ATP binding site were used during virtual screening. The protein structures were prepared using the Protein Preparation Wizard Workflow provided in the Maestro graphical user interface of the Schrödinger program suite and the default settings were used. Residues around the co-crystal ligands at a radius of 10 Å were defined as the binding region in which the docking grids were created. This radius was large enough to include all of the residues that may be involved in inhibitor binding. The crystallographic coordinates for each ligand (Vemurafenib and SB-590885) in the complex structure were extracted and designated as query templates in the ligand-based virtual screening.

Validation of the docking protocol

To evaluate the performance of various available docking methods (GLIDE 5.5,[53] GOLD 5.0,[62–64] AutoDock 4.2[65,66]) against B-Raf, two conventional criteria were employed during the pilot study. One of the measurements is the root mean-square deviation (RMSD) value between the best ranked pose predicted by various docking programs and the corresponding experimental pose. The other refers to the enrichment factors, which is defined as the fraction of active compounds found in a certain percentage of ranking list divided by the fraction of the screened library.

GLIDE 5.5. GLIDE (grid-based ligand docking with energetics) approximates a complete systematic search of chemical space available to the docked ligand.[53] In this search, an initial rough positioning and scoring phase that dramatically narrows down the search space is used to locate promising ligand poses. The conformational energy for a few hundred surviving candidate poses is then torsionally flexible minimized at the receptor environment with the OPLS-AA force field.[67] Monte Carlo simulation is finally conducted between the three to six lowest energy poses of the previous step to explore nearby torsional minima, which is critical for obtaining an accurate docked pose.

GOLD 5.0. GOLD performs automated molecular docking which employs the hydrogen bond-encoded genetic algorithm (GA) to direct the identification of proper binding modes.[62–64] A maximum of 10 000 genetic operations were performed on a set of five islands for each of the 20 independent GA runs. The default weights for three genetic operators (crossover, mutation and migration) and a population size of 100 chromosomes were applied in each docking simulation. The kinase scoring function[68] implemented in GOLD were utilized to rank the docked compounds, respectively. Early termination was allowed when the RMSD values for the top three scoring poses was less than 1.5 Å.

AutoDock 4.2. AutoDock Tools (ADT) was used to prepare the grid parameter files (gpf) and the docking parameter files (dpf) for each of the docked compound. A grid spacing of 0.375 Å was applied for the energetic map calculations, which centered on the co-crystal ligands and with the grid number of 60, 60, 60 in the *x*, *y*, and *z* directions. The Lamarckian genetic algorithm (LGA) was employed to explore the optimal chemical space in the ATP binding site for each ligand.[65] The docked compounds were subjected to 10 GA runs with a maximal energy evaluation number of 250 000 and a maximum of 27 000 generations. Default values were used for the other parameters and an RMSD tolerance of 2.0 Å was defined during the cluster analysis.

Virtual screening

The SHAFTS program was employed to perform the 3D molecular similarity based virtual screening. It adopts a hybrid similarity metric of molecular shape and pharmacophore features for 3D similarity calculation and ranking, aiming to combine the strength of both pharmacophore matching and volumetric overlay.[50] SHAFTS had demonstrated satisfactory active compounds enrichment and scaffold hopping capability against several representative kinases in retrospective virtual screening studies as well as recent prospective applications.[51,52] Taking the crystallographic conformation of Vemurafenib and SB-590885 in B-Raf/ligand complex as query templates, the conformational ensembles for each compound in the SPECS database were searched by SHAFTS, and only the best ranked conformer was reserved per molecule. The top 1000 molecules with similarity score >1.0 were reserved for each template. We employed the GLIDE program as the secondary filter to prioritize the compounds for experimental assessment. All of the candidate compounds derived from SHAFTS screening were docked into the ATP binding site of B-Raf without any constraint. The hit compounds were ranked based on G-score and the top ranking

 This journal is © The Royal Society of Chemistry 2012

compounds were submitted for further docking validation with the extra precision (XP) mode to eliminate false positives as accomplished by more extensive sampling and advanced scoring, resulting in even higher enrichment. Finally, after visual inspection and chemical diversity analysis, the candidate compounds were purchased and subject to the *in vitro* kinase inhibition assay.

Cloning, protein expression and purification

The human B-Raf kinase domain and the V600E containing mutant (B-Raf^{WT} and B-Raf^{V600E}, residues 433–726) with an N-terminal 6X-His tag (MDRGSH$_6$GS) to facilitate protein purification (in the presence of full-length mouse p50cdc37 to facilitate the proper folding of the B-Raf kinase) was expressed in Sf9 cells and purified to homogeneity as previously described.[39] The protein was stored at 1.5 mg mL^{-1} at 4 °C until use. GST-MEK-His protein substrate for the B-Raf inhibitor screen was over expressed at 37 °C in *Escherichia coli* BL21 (Gold) cells. The protein was stored at 10 mg mL^{-1} at −80 °C until use.

In vitro B-Raf kinase assay

For IC_{50} calculations of inhibitors, an ELISA-based assay was employed as previously described[39] at different inhibitor concentrations to generate a sigmoidal dose response curve using B-Raf^{V600E} or B-Raf^{WT} protein. All dose response measurements were carried out in duplicate or triplicate and IC_{50} values were derived from fitting the data to a sigmoidal dose response curve with a four-parameter logistic model using GraphPad Prism.

Melanoma proliferation assay

Human melanoma cell lines (A375, WM983B, 1205Lu, WM3918) were isolated as previously described[69] and cultured in Dulbecco's modified Eagle's medium supplemented with 5% fetal bovine serum. Normal human primary fibroblasts (FF2508) were isolated from the human epidermis of neonatal foreskins and cultured as described.[70,71] Cells (5000/well) were seeded in 96-well plates and allowed to adhere overnight before treatment with each compound or the DMSO vehicle control for 72 h. Cells were then directly incubated with MTS substrate (CellTiter-96 Aqueous One Solution Cell Proliferation Assay, Promega). Absorbance was measured at 490 nm as per the supplier's instructions and percent proliferation was normalized to the absorbance of vehicle-treated cells. For each experiment, cell line, and treatment, the absorbance values of at least 4 wells were used for data analysis and the experiment was conducted in triplicate.

Kinase profiling

Kinase profiling was performed at Shanghai ChemPartner Co., Ltd. according to the manufacturer's protocols. ATP concentrations in the kinase assay were at the K_m for each enzyme.

Chemistry: General methods

The reagents (chemicals) were purchased from Alfa Aesar, Sigma, Acros and Shanghai Chemical Reagent Company, and used without further purification. Column chromatography was performed with CombiFlash® Companion system (Teledyne Isco, Inc.). Nuclear magnetic resonance (NMR) spectra were performed on a Brucker AMX-400 and AMX-300 NMR (IS as TMS). Chemical shifts were reported in parts per million (ppm, δ) downfield from tetramethylsilane. Proton coupling patterns were described as singlet (s), doublet (d), triplet (t), quartet (q), multiplet (m), and broad (br). Low- and high-resolution mass spectra (LRMS and HRMS) were given with electric ionization (EI) produced by a Finnigan MAT-95. Melting points (Mp) are uncorrected and were measured in open capillary tubes, using a SGW X-4 melting point apparatus (−50 to 400 °C). An Agilent 1100 series HPLC with an Agilent Eclipse XDB-C18 (4.6 × 150 mm, 5 μm) reversed phase column was used for the HPLC analyses. The elution buffer was a mixture of H_2O–MeCN = 40 : 60 (v/v) with 0.1% CF3COOH (v/v) as an additive. The retention time of each synthesized compound is given and the corresponding purity for each compound is proved to be >95% by both HPLC test and ^{1}H-NMR Spectral Scan (see in the ESI†). The purity of compounds from the SPECS database is more than 90% and for most compounds greater than 95% (confirmed by SPECS, using NMR or LC−MS; data available through the web site).

General procedure for the synthesis of compounds

(a) General procedure for the synthesis of compound 30 *via* the Suzuki reaction. To a solution of 5-formyl-2-furanboronic acid (5.0 mmol) in a mixture (7/3) of dry toluene and ethanol (10 mL), various substituted bromobenzene (1.0 equiv), $Pd(PPh_3)_4$ (0.1 equiv) and K_2CO_3 (2.0 equiv) was added. The mixture was stirred and heated at 100 °C for 4 h under argon protection before it was cooled to room temperature. The organic solvents were removed under vacuum, and the residue was extracted with CH_2Cl_2 (3 × 50 mL) and washed with brine. The organic phase was finally dried over Na_2SO_4 and evaporated to dryness to give a crude compound that was purified through flash chromatography (ethyl acetate/petroleum ether) to yield compound **30**.

(b) General procedure for the synthesis of target compound. (i) **16a–g** and **17a–f**: a mixture of compound **30** (1.0 mmol), substituted 1-indanone or 2,3-dihydroindol-2-one (2.0 equiv) and NaOH (3.0 equiv) in MeOH was stirred and heated at room temperature for 3–4 h. The precipitate was obtained by filtration. The solid was re-crystallized with EtOH to yield pure product.

(ii) **19a–k**[72]: a mixture of compound **30** (1.0 mmol), 2,4-thiazolidinedione (2.0 equiv) and β-alanine (2.0 equiv) in acetic acid was stirred and heated at 90 °C for 2 h before it was cooled to room temperature. The precipitate was obtained by filtration. The solid was washed with MeOH to yield pure product without further purification.

(iii) **22a–q**[73]: a mixture of compound **30** (1.0 mmol) and 2-thiobarbituric acid (1.0 equiv) in acetic acid was stirred and

Published on 13 July 2012 on http://pubs.rsc.org | doi:10.1039/C2OB26081F
Downloaded by University of California - San Diego on 01 September 2012

Published on 13 July 2012 on http://pubs.rsc.org | doi:10.1039/C2OB26081F
Downloaded by University of California - San Diego on 01 September 2012

heated at 90 °C for 2 h before it was cooled to room temperature. The precipitate was obtained by filtration. The solid was washed with MeOH to yield pure product without further purification.

2-[5-(2-Nitro-phenyl)-furan-2-ylmethylene]-indan-1-one (16a). ^{1}H NMR (400 MHz, DMSO) δ 8.00 (dd, J = 10.8, 8.3 Hz, 2H), 7.83–7.75 (m, 2H), 7.72 (d, J = 7.4 Hz, 1H), 7.70–7.60 (m, 2H), 7.50 (d, J = 7.4 Hz, 1H), 7.36 (s, 1H), 7.26 (q, J = 3.7 Hz, 2H), 3.95 (s, 2H). Mp 147–148 °C. LRMS (EI) m/z 331, M^+. HRMS (EI) m/z calcd $C_{20}H_{13}NO_4$ M^+ 331.0845, found 331.0844.

2-[5-(3-Trifluoromethyl-phenyl)-furan-2-ylmethylene]-indan-1-one (16b). ^{1}H NMR (400 MHz, DMSO) δ 8.19–8.17 (m, 2H), 7.77–7.71 (m, 5H), 7.50–7.48 (d, J = 3.7 Hz, 2H), 7.41–7.40 (s, 1H), 7.25–7.24 (d, J = 3.7 Hz, 1H), 4.17 (s, 2H). Mp 171–173 °C. LRMS (EI) m/z 354, M^+. HRMS (EI) m/z calcd $C_{21}H_{13}F_3O_2$ M^+ 354.0868, found 354.0867.

2-[5-(3-Trifluoromethyl-phenyl)-furan-2-ylmethylene]-5-chloro-indan-1-one (16c). ^{1}H NMR (400 MHz, DMSO) δ 8.28 (s, 1H), 7.89 (d, J = 8.4 Hz, 1H), 7.83–7.76 (m, 2H), 7.71 (s, 1H), 7.59–7.47 (m, 3H), 7.31 (d, J = 3.8 Hz, 1H), 4.17 (s, 2H). Mp 220–221 °C. LRMS (EI) m/z 388, M^+. HRMS (EI) m/z calcd $C_{21}H_{12}ClF_3O_2$ M^+ 388.0478, found 388.0475.

2-[5-(4-Nitro-phenyl)-furan-2-ylmethylene]-indan-1-one (16d). ^{1}H NMR (400 MHz, DMSO) δ 8.36 (d, J = 8.5 Hz, 2H), 8.14 (d, J = 8.6 Hz, 2H), 7.81–7.70 (m, 3H), 7.54 (d, J = 32.1 Hz, 2H), 7.43 (s, 1H), 7.31 (s, 1H), 4.22 (s, 2H). Mp 224–225 °C. LRMS (EI) m/z 331, M^+. HRMS (EI) m/z calcd $C_{20}H_{13}NO_4$ M^+ 331.0845, found 331.0837.

2-[5-(4-Chloro-phenyl)-furan-2-ylmethylene]-indan-1-one (16e). ^{1}H NMR (400 MHz, DMSO) δ 7.89 (d, J = 8.6 Hz, 2H), 7.81–7.67 (m, 3H), 7.57 (d, J = 8.6 Hz, 2H), 7.53–7.46 (m, 1H), 7.38 (s, 1H), 7.29 (d, J = 3.6 Hz, 1H), 7.21 (d, J = 3.6 Hz, 1H), 4.15 (s, 2H). Mp 184–185 °C. LRMS (EI) m/z 320, M^+. HRMS (EI) m/z calcd $C_{20}H_{13}ClO_2$ M^+ 320.0604, found 320.0610.

2-[5-(4-Bromo-phenyl)-furan-2-ylmethylene]-indan-1-one (16f). ^{1}H NMR (400 MHz, DMSO) δ 7.82 (d, J = 8.6 Hz, 2H), 7.76 (d, J = 7.6 Hz, 1H), 7.74–7.70 (m, 3H), 7.69 (s, 1H), 7.52–7.44 (m, 1H), 7.38 (s, 1H), 7.30 (d, J = 3.6 Hz, 1H), 7.21 (d, J = 3.6 Hz, 1H), 4.14 (s, 2H). Mp 190–192 °C. LRMS (EI) m/z 364, M^+. HRMS (EI) m/z calcd $C_{20}H_{13}BrO_2$ M^+ 364.0099, found 320.0124.

2-[5-(2-Chloro-5-trifluoromethyl)-furan-2-ylmethylene]-indan-1-one (16g). ^{1}H NMR (400 MHz, DMSO) δ 8.28 (s, 1H), 7.87 (d, J = 8.4 Hz, 1H), 7.78 (d, J = 7.7 Hz, 2H), 7.72 (t, J = 7.4 Hz, 1H), 7.62 (d, J = 7.6 Hz, 1H), 7.50 (t, J = 5.3 Hz, 2H), 7.44 (s, 1H), 7.28 (d, J = 3.6 Hz, 1H), 4.14 (s, 2H). Mp 183–185 °C. LRMS (EI) m/z 388, M^+. HRMS (EI) m/z calcd $C_{21}H_{12}ClF_3O_2$ M^+ 388.0478, found 388.0482.

3-[5-(3-Trifluoromethyl-phenyl)-furan-2-ylmethylene]-1,3-dihydro-indol-2-one (17a). ^{1}H NMR (400 MHz, DMSO) δ 10.73 (s, 1H), 8.46 (d, J = 2.0 Hz, 1H), 8.22 (s, 2H), 7.78 (d, J = 8.1 Hz, 2H), 7.58 (d, J = 3.7 Hz, 1H), 7.49 (d, J = 3.7 Hz, 1H), 7.40 (s, 1H), 7.32 (dd, J = 8.3, 2.1 Hz, 1H), 6.90 (d, J = 8.3 Hz, 1H). Mp 206–207 °C. LRMS (EI) m/z 355, M^+. HRMS (EI) m/z calcd $C_{20}H_{12}F_3NO_2$ M^+ 355.0820, found 355.0820.

3-[5-(3-Trifluoromethyl-phenyl)-furan-2-ylmethylene]-6-chloro-1,3-dihydro-indol-2-one (17b). ^{1}H NMR (400 MHz, DMSO) δ 8.32 (d, J = 8.3 Hz, 1H), 8.13 (s, 2H), 7.76 (d, J = 5.8 Hz, 2H), 7.49 (d, J = 3.7 Hz, 1H), 7.39 (d, J = 3.7 Hz, 1H), 7.30 (s, 1H), 6.96 (dd, J = 8.3, 1.9 Hz, 1H), 6.87 (d, J = 1.9 Hz, 1H). Mp 226–228 °C. LRMS (EI) m/z 389, M^+. HRMS (EI) m/z calcd $C_{20}H_{11}ClF_3NO_2$ M^+ 389.0430, found 389.0427.

3-[5-(3-Trifluoromethyl-phenyl)-furan-2-ylmethylene]-5-chloro-1,3-dihydro-indol-2-one (17c). ^{1}H NMR (400 MHz, DMSO) δ 8.45 (dd, J = 7.7, 3.9 Hz, 1H), 8.25–8.11 (m, 2H), 7.78 (d, J = 4.1 Hz, 2H), 7.53 (dd, J = 6.3, 3.8 Hz, 1H), 7.42 (dd, J = 6.2, 2.7 Hz, 1H), 7.39–7.27 (m, 2H), 7.02 (td, J = 7.6, 3.1 Hz, 1H), 6.91 (d, J = 7.7 Hz, 1H). Mp 246–248 °C. LRMS (EI) m/z 389, M^+. HRMS (EI) m/z calcd $C_{20}H_{11}ClF_3NO_2$ M^+ 389.0430, found 389.0432.

3-[5-(2-Chloro-5-trifluoromethyl)-furan-2-ylmethylene]-1,3-dihydro-indol-2-one (17d). ^{1}H NMR (400 MHz, DMSO) δ 10.64 (s, 1H), 8.37 (dd, J = 8.8, 4.4 Hz, 2H), 7.91 (d, J = 8.4 Hz, 1H), 7.85–7.77 (m, 1H), 7.56 (d, J = 3.8 Hz, 1H), 7.47 (d, J = 3.8 Hz, 1H), 7.38 (s, 1H), 7.29 (d, J = 1.0 Hz, 1H), 6.90 (d, J = 7.8 Hz, 2H), 3.33 (s, 2H). Mp 207–208 °C. LRMS (EI) m/z 389, M^+. HRMS (EI) m/z calcd $C_{20}H_{11}ClF_3NO_2$ M^+ 389.0430, found 389.0430.

3-[5-(2-Chloro-5-trifluomethyl)-furan-2-ylmethylene]-5-chloro-1,3-dihydro-indol-2-one (17e). ^{1}H NMR (400 MHz, DMSO) δ 8.31 (d, J = 2.1 Hz, 1H), 8.26 (d, J = 1.7 Hz, 1H), 7.93 (dd, J = 12.2, 3.5 Hz, 1H), 7.85 (dd, J = 8.4, 2.2 Hz, 1H), 7.51 (dd, J = 11.4, 3.8 Hz, 2H), 7.43 (s, 1H), 7.30 (d, J = 2.1 Hz, 1H), 6.88 (d, J = 8.3 Hz, 1H). Mp 244–245 °C. LRMS (EI) m/z 423, M^+. HRMS (EI) m/z calcd $C_{20}H_{10}Cl_2F_3NO_2$ M^+ 423.0041, found 423.0042.

3-[5-(2-Chloro-5-trifluoromethyl)-furan-2-ylmethylene]-6-chloro-1,3-dihydro-indol-2-one (17f). ^{1}H NMR (400 MHz, DMSO) δ 10.80 (s, 1H), 8.32 (dd, J = 7.6, 5.1 Hz, 2H), 7.90 (t, J = 8.3 Hz, 1H), 7.85 (d, J = 2.2 Hz, 1H), 7.55 (d, J = 3.7 Hz, 1H), 7.50 (d, J = 3.8 Hz, 1H), 7.41 (s, 1H), 6.91 (d, J = 1.9 Hz, 1H), 6.87 (dd, J = 8.2, 1.9 Hz, 1H). Mp 286–287 °C. LRMS (EI) m/z 423, M^+. HRMS (EI) m/z calcd $C_{20}H_{10}Cl_2F_3NO_2$ M^+ 423.0041, found 423.0042.

5-[5-(2-Nitro-phenyl)-furan-2-ylmethylene]-thiazolidine-2,4-dione (19a). ^{1}H NMR (400 MHz, DMSO) δ 12.51 (s, 1H), 8.00–7.98 (d, J = 8.0 Hz, 1H), 7.93–7.91 (d, J = 8.0 Hz, 1H), 7.81–7.79 (t, J = 8.0 Hz, 1H), 7.69–7.65 (t, J = 8.0 Hz, 1H), 7.61 (s, 1H), 7.25–7.24 (d, J = 4.0 Hz, 1H), 7.20–7.19 (d, J = 4.0 Hz, 1H). Mp 250–252 °C. LRMS (EI) m/z 316, M^+. HRMS (EI) m/z $C_{14}H_8N_2O_5S$ M^+, calcd 316.0154, found 316.0153.

5-[5-(3-Methoxy-phenyl)-furan-2-ylmethylene]-thiazolidine-2,4-dione (19b). ^{1}H NMR (400 MHz, DMSO) δ 12.50 (s, 1H), 7.65 (s, 1H), 7.47–7.43 (t, J = 7.9 Hz, 1H), 7.42–7.39 (d, J = 7.9 Hz, 1H), 7.35 (s, 1H), 7.33–7.32 (d, J = 4.0 Hz, 1H), 7.24–7.23 (d, J = 4.0 Hz, 1H), 3.83 (s, 3H). Mp 222–223 °C. LRMS (EI) m/z 301, M^+. HRMS (EI) m/z $C_{15}H_{11}NO_4S$ M^+, calcd 301.0409, found 301.0409.

5-[5-(4-Nitro-phenyl)-furan-2-ylmethylene]-thiazolidine-2,4-dione (19c). ^{1}H NMR (400 MHz, DMSO) δ 12.53 (s, 1H),

 This journal is © The Royal Society of Chemistry 2012

Downloaded by University of California - San Diego on 01 September 2012
Published on 13 July 2012 on http://pubs.rsc.org | doi:10.1039/C2OB26081F

8.31–8.29 (d, J = 8.1 Hz, 2H), 7.95–7.93 (d, J = 8.1 Hz, 2H), 7.59 (s, 1H), 7.51–7.50 (d, J = 4.0 Hz, 1H), 7.24–7.22 (d, J = 4.0 Hz, 1H)). Mp 330–331 °C. LRMS (EI) m/z 316, M^+. HRMS (EI) m/z $C_{14}H_8N_2O_5S$ M^+, calcd 316.0154, found 316.0149.

4-{5-[(2,4-Dioxo-thiazolidin-5-ylidene)methyl]-furan-2-yl}benzoic acid ethyl ester (19d). ^{1}H NMR δ (400 MHz, DMSO) δ 12.52 (s, 1H), 8.07–8.04 (d, J = 8.6 Hz, 2H), 7.92–7.89 (d, J = 8.6 Hz, 2H), 7.64 (s, 1H), 7.43–7.42 (d, J = 3.6 Hz, 1H), 7.24–7.23 (d, J = 3.6 Hz, 1H), 4.35–4.30 (q, J = 7.0 Hz, 2H), 1.35–1.32 (t, J = 7.0 Hz, 3H). Mp 259–261 °C. LRMS (EI) m/z 343, M^+. HRMS (EI) m/z $C_{17}H_{13}NO_5S$ M^+, calcd 343.0514, found 343.0513.

5-[5-(4-Chloro-phenyl)-furan-2-ylmethylene]-thiazolidine-2,4-dione (19e). ^{1}H NMR (400 MHz, DMSO) δ 12.49 (b, 1H), 7.83–7.80 (d, J = 8.1 Hz, 2H), 7.61–7.57 (m, 3H), 7.32–7.30 (d, J = 3.8 Hz, 1H), 7.22–7.21 (d, J = 3.8 Hz, 1H). Mp 279–280 °C. LRMS (EI) m/z 305, M^+. HRMS (EI) m/z $C_{14}H_8ClNO_3S$ M^+, calcd 304.9913, found 304.9920.

5-[5-(4-Methyl-phenyl)-furan-2-ylmethylene]-thiazolidine-2,4-dione (19g). ^{1}H NMR (400 MHz, DMSO) δ 12.44 (s, 1H), 7.71–7.69 (d, J = 8.1 Hz, 2H), 7.61 (s, 1H), 7.34–7.32 (d, J = 8.1 Hz, 2H), 7.21–7.19 (m, 2H), 2.34 (s, 3H). Mp 262–264 °C. LRMS (EI) m/z 285, M^+. HRMS (EI) m/z $C_{15}H_{11}NO_3S$ M^+, calcd 285.0460, found 285.0466.

5-[5-(4-Methoxy-phenyl)-furan-2-ylmethylene]-thiazolidine-2,4-dione (19h). ^{1}H NMR (400 MHz, DMSO) δ 12.41 (s, 1H), 7.77–7.72 (d, J = 8.8 Hz, 2H), 7.61 (s, 1H), 7.20–7.18 (d, J = 3.6 Hz, 1H), 7.12–7.06 (m, 3H), 3.79 (s, 3H). Mp 272 °C. LRMS (EI) m/z 301, M^+. HRMS (EI) m/z $C_{15}H_{11}NO_4S$ M^+, calcd 301.0409, found 301.0404.

5-[5-(4-*tert*-Butyl-phenyl)-furan-2-ylmethylene]-thiazolidine-2,4-dione (19i). ^{1}H NMR (400 MHz, DMSO) δ 12.44 (s, 1H), 7.75–7.72 (d, J = 8.1 Hz, 2H), 7.62 (s, 1H), 7.55–7.52 (d, J = 8.1 Hz, 2H), 7.21–7.19 (m, 2H), 1.29 (s, 3H). Mp 275–277 °C. LRMS (EI) m/z 327, M^+. HRMS (EI) m/z $C_{18}H_{17}NO_3S$ M^+, calcd 327.0929, found 327.0928.

5-[5-(2-Naphthyl)-furan-2-ylmethylene]-thiazolidine-2,4-dione (19j). ^{1}H NMR (400 MHz, DMSO) δ 12.51 (s, 1H), 8.32 (s, 1H), 8.06–8.03 (m, 2H), 7.96–7.94 (d, J = 8.0 Hz, 2H), 7.67 (s, 1H), 7.60–7.54 (m, 2H), 7.42–7.41 (d, J = 4.0 Hz, 1H), 7.29–7.28 (d, J = 4.0 Hz, 1H). Mp 246–247 °C. LRMS (EI) m/z 321, M^+. HRMS (EI) m/z $C_{18}H_{11}NO_3S$ M^+, calcd 321.0460, found 321.0462.

5-[5-(2-Chloro-5-trifluomethyl)-furan-2-ylmethylene]-thiazolidine-2,4-dione (19k). ^{1}H NMR (400 MHz, DMSO) δ 12.57 (s, 1H), 8.12 (s, 1H), 7.85–7.83 (d, J = 8.5 Hz, 2H), 7.77–7.75 (d, J = 8.5 Hz, 2H), 7.66 (s, 1H), 7.52–7.51 (d, J = 3.8 Hz, 1H), 7.26–7.25 (d, J = 3.8 Hz, 1H). Mp 259 °C. LRMS (EI) m/z 373, M^+. HRMS (EI) m/z $C_{18}H_{11}NO_3S$ M^+, calcd 372.9787, found 372.9791.

5-[5-(2-Nitro-phenyl)-furan-2-ylmethylene]-2-thioxo-dihydro-pyrimidine-4,6-dione (22a). ^{1}H NMR (400 MHz, DMSO) δ 12.51 (s, 1H), 12.45 (s, 1H), 8.61–8.60 (d, J = 4.0 Hz, 1H), 8.09–8.03 (t, J = 8.3 Hz, 2H), 7.89 (s, 1H), 7.88–7.83 (t, J = 8.3 Hz, 1H), 7.78–7.74 (t, J = 8.3 Hz, 1H), 7.42–7.40 (d, J = 4.0 Hz, 1H). Mp 302–303 °C. LRMS (EI) m/z 343, M^+. HRMS (EI) m/z $C_{15}H_9N_3O_5S$ M^+, calcd 343.0263, found 343.0272.

5-[5-(3-Methoxy-phenyl)-furan-2-ylmethylene]-2-thioxo-dihydro-pyrimidine-4,6-dione (22b). ^{1}H NMR (400 MHz, DMSO) δ 12.43 (s, 1H), 12.37 (s, 1H), 8.62–8.61 (d, J = 4.0 Hz, 1H), 8.11 (s, 1H), 7.57–7.51 (m, 3H), 7.46–7.42 (d, J = 8.4 Hz, 1H), 7.07–7.04 (d, J = 8.4 Hz, 1H), 3.83 (s, 3H). Mp 335–336 °C. LRMS (EI) m/z 328, M^+. HRMS (EI) m/z $C_{16}H_{12}N_2O_4S$ M^+, calcd 328.0518, found 328.0515.

5-[5-(4-Nitro-phenyl)-furan-2-ylmethylene]-2-thioxo-dihydro-pyrimidine-4,6-dione (22c). ^{1}H NMR (400 MHz, DMSO) δ 12.50 (s, 1H), 12.44 (s, 1H), 8.60–8.58 (d, J = 4.0 Hz, 1H), 8.48–8.35 (d, J = 8.5 Hz, 2H), 8.24–8.21 (d, J = 8.6 Hz, 2H), 8.12 (s, 1H), 7.74–7.72 (d, J = 4.0 Hz, 1H). Mp 329–330 °C. LRMS (EI) m/z 343, M^+. HRMS (EI) m/z calcd $C_{15}H_9N_3O_5S$ M^+ 343.0263, found 343.0272.

5-[5-(4-Chloro-phenyl)-furan-2-ylmethylene]-2-thioxo-dihydro-pyrimidine-4,6-dione (22e). ^{1}H NMR (400 MHz, DMSO) δ 12.44 (s, 1H), 12.38 (s, 1H), 8.61–8.60 (d, J = 4.0 Hz, 1H), 8.11 (s, 1H), 8.03–7.99 (d, J = 8.6 Hz, 2H), 7.63–7.60 (d, J = 8.6 Hz, 2H), 7.55–7.53 (d, J = 4.0 Hz, 1H). Mp 317–318 °C. LRMS (EI) m/z 332, M^+. HRMS (EI) m/z $C_{15}H_9ClN_2O_3S$ M^+, calcd 332.0022, found 332.0018.

5-[5-(4-Bromo-phenyl)-furan-2-ylmethylene]-2-thioxo-dihydro-pyrimidine-4,6-dione (22f). ^{1}H NMR (400 MHz, DMSO) δ 12.44 (s, 1H), 12.38 (s, 1H), 8.59–8.58 (d, J = 4.0 Hz, 1H), 8.09 (s, 1H), 7.94–7.90 (d, J = 8.6 Hz, 2H), 7.75–7.72 (d, J = 8.6 Hz, 2H), 7.54–7.53 (d, J = 4.0 Hz, 1H). Mp 327–328 °C. LRMS (EI) m/z 376, M^+. HRMS (EI) m/z $C_{15}H_9BrN_2O_3S$ M^+, calcd 375.9517, found 375.9519.

5-[5-(4-Methyl-phenyl)-furan-2-ylmethylene]-2-thioxo-dihydro-pyrimidine-4,6-dione (22g). ^{1}H NMR (400 MHz, DMSO) δ 12.35 (s, 1H), 12.28 (s, 1H), 8.62–8.61 (d, J = 4.1 Hz, 1H), 8.09 (s, 1H), 7.88–7.86 (d, J = 8.1 Hz, 2H), 7.43–7.42 (d, J = 4.1 Hz, 2H), 7.35–7.33 (d, J = 8.1 Hz, 1H), 2.36 (s, 3H). Mp 335 °C. LRMS (EI) m/z 312, M^+. HRMS (EI) m/z $C_{16}H_{12}N_2O_3S$ M^+, calcd 312.0569, found 312.0572.

5-[5-(4-Methoxy-phenyl)-furan-2-ylmethylene]-2-thioxo-dihydro-pyrimidine-4,6-dione (22h). ^{1}H NMR (400 MHz, DMSO) δ 12.36 (s, 1H), 12.30 (s, 1H), 8.64–8.63 (d, J = 4.0 Hz, 1H), 8.07 (s, 1H), 7.95–7.90 (d, J = 8.5 Hz, 2H), 7.39–7.37 (d, J = 4.0 Hz, 1H), 7.11–7.06 (d, J = 8.5 Hz, 2H), 3.83 (s, 3H). Mp 346–347 °C. LRMS (EI) m/z 328, M^+. HRMS (EI) m/z $C_{16}H_{12}N_2O_4S$ M^+, calcd 328.0518, found 328.0517.

5-[5-(4-*tert*-Butyl-phenyl)-furan-2-ylmethylene]-2-thioxo-dihydro-pyrimidine-4,6-dione (22i). ^{1}H NMR (400 MHz, DMSO) δ 12.40 (s, 1H), 12.35 (s, 1H), 8.64–8.63 (d, J = 4.1 Hz, 1H), 8.09 (s, 1H), 7.92–7.90 (d, J = 8.6 Hz, 2H), 7.56–7.53 (d, J = 8.6 Hz, 2H), 7.46–7.45 (d, J = 4.1 Hz, 1H), 1.29 (s, 9H). Mp 303–304 °C. LRMS (EI) m/z 354, M^+. HRMS (EI) m/z $C_{19}H_{18}N_2O_3S$ M^+, calcd 354.1038, found 354.1036.

5-[5-(2-Naphthyl)-furan-2-ylmethylene]-2-thioxo-dihydro-pyrimidine-4,6-dione (22j). ^{1}H NMR (400 MHz, DMSO) δ 12.45 (s, 1H), 12.39 (s, 1H), 8.69–8.68 (d, J = 4.0 Hz, 1H), 8.59 (s,

1H), 8.16 (s, 1H), 8.09–8.04 (m, 3H), 7.97 (s, 1H), 7.64–7.59 (m, 3H). Mp 352–354 °C. LRMS (EI) *m/z* 348, M^+. HRMS (EI) *m/z* $C_{19}H_{12}N_2O_3S$ M^+, calcd 348.0569, found 348.0569.

5-[5-(2-Chloro-5-trifluoromethyl)-furan-2-ylmethylene]-2-thioxo-dihydro-pyrimidine-4,6-dione (22k). ^{1}H NMR (400 MHz, DMSO) δ 12.49 (s, 1H), 12.44 (s, 1H), 8.59–8.58 (d, J = 4.0 Hz, 1H), 8.45 (s, 1H), 8.19 (s, 1H), 7.90–7.85 (d, J = 8.5 Hz, 1H), 7.84–7.82 (d, J = 8.5 Hz, 1H), 7.70–7.69 (d, J = 4.0 Hz, 1H). Mp 360–362 °C. LRMS (EI) *m/z* 400, M^+. HRMS (EI) *m/z* $C_{18}H_6ClF_3N_2O_3S$ M^+, calcd 399.9896, found 399.9857.

5-[5-(3-Trifluoromethyl-phenyl)-furan-2-ylmethylene]-2-thioxo-dihydro-pyrimidine-4,6-dione (22l). ^{1}H NMR (400 MHz, DMSO) δ 12.46 (s, 1H), 12.41 (s, 1H), 8.62–8.61 (d, J = 4.0 Hz, 1H), 8.33 (s, 1H), 8.29–8.27 (d, J = 8.4 Hz, 1H), 8.16 (s, 1H), 7.83–7.85 (d, J = 8.4 Hz, 1H), 7.80–7.76 (t, J = 8.4 Hz, 1H), 7.70–7.69 (d, J = 4.0 Hz, 1H). Mp 302–303 °C. LRMS (EI) *m/z* 366, M^+. HRMS (EI) *m/z* $C_{16}H_{19}F_3N_2O_3S$ M^+, calcd 366.0286, found 366.0284.

4-[5-(4,6-Dioxo-2-thioxo-tetrahydro-pyrimidin-5-ylidene-methyl)furan-2-yl]benzoic acid (22m). ^{1}H NMR (400 MHz, DMSO) δ 12.46 (s, 1H), 12.40 (s, 1H), 8.62–8.61 (d, J = 4.1 Hz, 1H), 8.11–8.03 (m, 5H), 7.63–7.62 (d, J = 4.1 Hz, 1H). Mp >400 °C. LRMS (EI) *m/z* 342, M^+. HRMS (EI) *m/z* $C_{16}H_{10}N_2O_5S$ M^+, calcd 342.0301, found 342.0311.

5-[5-(2-Nitro-4-chloro)-furan-2-ylmethylene]-2-thioxo-dihydro-pyrimidine-4,6-dione (22n). ^{1}H NMR (400 MHz, DMSO) δ 12.49 (s, 1H), 12.43 (s, 1H), 8.59–8.58 (d, J = 4.0 Hz, 1H), 8.26 (s, 1H), 8.11–8.09 (d, J = 8.4 Hz, 1H), 7.94–7.92 (d, J = 8.4 Hz, 1H), 7.86 (s, 1H), 7.42–7.41 (d, J = 4.0 Hz, 1H). Mp 300–301 °C. LRMS (EI) *m/z* 377, M^+. HRMS (EI) *m/z* $C_{15}H_8ClN_3O_5S$ M^+, calcd 376.9873, found 376.9884.

5-[5-(2-Trifluoromethyl-4-chloro)-furan-2-ylmethylene]-2-thioxo-dihydro-pyrimidine-4,6-dione (22o). ^{1}H NMR (400 MHz, DMSO) 12.49 (s, 1H), 12.43 (s, 1H), 8.62–8.60 (d, J = 4.0 Hz, 1H), 8.08–8.06 (d, J = 8.4 Hz, 1H), 8.03 (s, 1H), 8.00 (s, 1H), 7.94–7.92 (d, J = 8.4 Hz, 1H), 7.36–7.35 (d, J = 4.0 Hz, 1H). Mp 325–326 °C. LRMS (EI) *m/z* 400, M^+. HRMS (EI) *m/z* $C_{16}H_8ClF_3N_2O_3S$ M^+, calcd 399.9896, found 399.9857.

5-[5-(3-Trifluoromethyl-4-chloro)-furan-2-ylmethylene]-2-thioxo-dihydro-pyrimidine-4,6-dione (22p). ^{1}H NMR (400 MHz, DMSO) δ 12.47 (s, 1H), 12.43 (s, 1H), 8.57–8.56 (d, J = 4.0 Hz, 1H), 8.35 (s, 1H), 8.26–8.23 (d, J = 8.4 Hz, 1H), 8.12 (s, 1H), 7.89–7.87 (d, J = 8.4 Hz, 1H), 7.70–7.69 (d, J = 4.0 Hz, 1H). Mp 323–325 °C. LRMS (EI) *m/z* 400, M^+. HRMS (EI) *m/z* $C_{16}H_8ClF_3N_2O_3S$ M^+, calcd 399.9896, found 399.9869.

5-[5-(3,4-Methylenedioxy)-furan-2-ylmethylene]-2-thioxo-dihydro-pyrimidine-4,6-dione (22q). ^{1}H NMR (400 MHz, DMSO) δ 12.39 (s, 1H), 12.33 (s, 1H), 8.63–8.62 (d, J = 4.0 Hz, 1H), 8.10 (s, 1H), 7.59–7.56 (m, 2H), 7.42–7.41 (d, J = 4.0 Hz, 1H), 7.11–7.09 (d, J = 8.5 Hz, 1H), 6.14 (s, 2H). Mp >400 °C. LRMS (EI) *m/z* 342, M^+. HRMS (EI) *m/z* $C_{16}H_{10}N_2O_5S$ M^+, calcd 342.0310, found 342.0302.

Published on 13 July 2012 on http://pubs.rsc.org | doi:10.1039/C2OB26081F
Downloaded by University of California - San Diego on 01 September 2012

Acknowledgements

We gratefully acknowledge financial support from the National Institutes of Health (NIH) to RM and MH (CA114046). We also gratefully acknowledge financial support from the State Key Program of Basic Research of China grant to HJ (2009CB918502), the National Natural Science Foundation of China grants to CL (20972174 and 91029704), HJ (21021063) and HL (81025017), National S&T Major Projects to HL (2012ZX09103-101-072), National High Technology Research and Development Program of China (2012AA020302) and the Chinese Academy of Sciences (XDA01040305) grant to CL.

References

1 R. Seger and E. G. Krebs, *FASEB J.*, 1995, **9**, 726–735.
2 M. J. Robinson and M. H. Cobb, *Curr. Opin. Cell Biol.*, 1997, **9**, 180–186.
3 H. Rubinfeld and R. Seger, *Mol. Biotechnol.*, 2005, **31**, 151–174.
4 E. K. Kim and E. J. Choi, *Biochim. Biophys. Acta, Mol. Basis Dis.*, 2010, **1802**, 396–405.
5 A. S. Dhillon, S. Hagan, O. Rath and W. Kolch, *Oncogene*, 2007, **26**, 3279–3290.
6 R. Hoshino, Y. Chatani, T. Yamori, T. Tsuruo, H. Oka, O. Yoshida, Y. Shimada, S. Ari-i, H. Wada, J. Fujimoto and M. Kohno, *Oncogene*, 1999, **18**, 813–822.
7 H. Davies, G. R. Bignell, C. Cox, P. Stephens, S. Edkins, S. Clegg, J. Teague, H. Woffendin, M. J. Garnett, W. Bottomley, N. Davis, N. Dicks, R. Ewing, Y. Floyd, K. Gray, S. Hall, R. Hawes, J. Hughes, V. Kosmidou, A. Menzies, C. Mould, A. Parker, C. Stevens, S. Watt, S. Hooper, R. Wilson, H. Jayatilake, B. A. Gusterson, C. Cooper, J. Shipley, D. Hargrave, K. Pritchard-Jones, N. Maitland, G. Chenevix-Trench, G. J. Riggins, D. D. Bigner, G. Palmieri, A. Cossu, A. Flanagan, A. Nicholson, J. W. C. Ho, S. Y. Leung, S. T. Yuen, B. L. Weber, H. F. Siegler, T. L. Darrow, H. Paterson, R. Marais, C. J. Marshall, R. Wooster, M. R. Stratton and P. A. Futreal, *Nature*, 2002, **417**, 949–954.
8 H. Rajagopalan, A. Bardelli, C. Lengauer, K. W. Kinzler, B. Vogelstein and V. E. Velculescu, *Nature*, 2002, **418**, 934.
9 U. R. Rapp, J. Fensterle, S. Albert and R. Gotz, *Adv. Enzyme Regul.*, 2003, **43**, 183–195.
10 R. Mukherjee, J. M. Bartlett, N. S. Krishna, M. A. Underwood and J. Edwards, *Prostate*, 2005, **64**, 101–107.
11 C. Damodar Reddy, S. Marwaha, R. Patti, M. Raghunath, A. C. Duhaime, L. Sutton and P. C. Phillips, *Anticancer Res.*, 2001, **21**, 2733–2738.
12 N. Giuliani, P. Lunghi, F. Morandi, S. Colla, S. Bonomini, M. Hojden, V. Rizzoli and A. Bonati, *Leukemia*, 2004, **18**, 628–635.
13 J. A. McCubrey, L. S. Steelman, W. H. Chappell, S. L. Abrams, E. W. Wong, F. Chang, B. Lehmann, D. M. Terrian, M. Milella, A. Tafuri, F. Stivala, M. Libra, J. Basecke, C. Evangelisti, A. M. Martelli and R. A. Franklin, *Biochim. Biophys. Acta, Mol. Cell Res.*, 2007, **1773**, 1263–1284.
14 L. S. Steelman, S. L. Abrams, J. G. Shelton, W. H. Chappell, J. Basecke, F. Stivala, M. Donia, F. Nicoletti, M. Libra, A. M. Martelli and J. A. McCubrey, *Cell Cycle*, 2010, **9**, 1629–1638.
15 J. S. Sebolt-Leopold and R. Herrera, *Nat. Rev. Cancer*, 2004, **4**, 937–947.
16 P. J. Roberts and C. J. Der, *Oncogene*, 2007, **26**, 3291–3310.
17 J. A. Gollob, S. Wilhelm, C. Carter and S. L. Kelley, *Semin. Oncol.*, 2006, **33**, 392–406.
18 A. Zebisch and J. Troppmair, *Cell. Mol. Life Sci.*, 2006, **63**, 1314–1330.
19 R. Roskoski Jr., *Biochem. Biophys. Res. Commun.*, 2010, **399**, 313–317.
20 D. T. Leicht, V. Balan, A. Kaplun, V. Singh-Gupta, L. Kaplun, M. Dobson and G. Tzivion, *Biochim. Biophys. Acta, Mol. Cell Res.*, 2007, **1773**, 1196–1212.
21 H. Chong, H. G. Vikis and K. L. Guan, *Cell. Signalling*, 2003, **15**, 463–469.
22 K. E. Mercer and C. A. Pritchard, *Biochim. Biophys. Acta*, 2003, **1653**, 25–40.
23 C. A. Pritchard, M. L. Samuels, E. Bosch and M. McMahon, *Mol. Cell. Biol.*, 1995, **15**, 6430–6442.

This journal is © The Royal Society of Chemistry 2012

View Online

Downloaded by University of California - San Diego on 01 September 2012
Published on 13 July 2012 on http://pubs.rsc.org | doi:10.1039/C2OB26081F

24 C. S. Mason, C. J. Springer, R. G. Cooper, G. Superti-Furga, C. J. Marshall and R. Marais, *EMBO J.*, 1999, **18**, 2137–2148.
25 S. A. Moodie, M. J. Paris, W. Kolch and A. Wolfman, *Mol. Cell. Biol.*, 1994, **14**, 7153–7162.
26 L. Wojnowski, L. F. Stancato, A. C. Larner, U. R. Rapp and A. Zimmer, *Mech. Dev.*, 2000, **91**, 97–104.
27 M. Garnett and R. Marais, *Cancer Cell*, 2004, **6**, 313.
28 C. Wellbrock and A. Hurlstone, *Biochem. Pharmacol.*, 2010, **80**, 561–567.
29 P. T. Wan, M. J. Garnett, S. M. Roe, S. Lee, D. Niculescu-Duvaz, V. M. Good, C. M. Jones, C. J. Marshall, C. J. Springer, D. Barford and R. Marais, *Cell*, 2004, **116**, 855–867.
30 C. A. Pratilas, B. S. Taylor, Q. Ye, A. Viale, C. Sander, D. B. Solit and N. Rosen, *Proc. Natl. Acad. Sci. U. S. A.*, 2009, **106**, 4519–4524.
31 C. Wellbrock, M. Karasarides and R. Marais, *Nat. Rev. Mol. Cell Biol.*, 2004, **5**, 875–885.
32 R. Houben, J. C. Becker, A. Kappel, P. Terheyden, E. B. Brocker, R. Goetz and U. R. Rapp, *J. Carcinog.*, 2004, **3**, 6.
33 W. S. Samowitz, C. Sweeney, J. Herrick, H. Albertsen, T. R. Levin, M. A. Murtaugh, R. K. Wolff and M. L. Slattery, *Cancer Res.*, 2005, **65**, 6063–6069.
34 L. Liu, Y. Cao, C. Chen, X. Zhang, A. McNabola, D. Wilkie, S. Wilhelm, M. Lynch and C. Carter, *Cancer Res.*, 2006, **66**, 11851–11858.
35 A. J. King, D. R. Patrick, R. S. Batorsky, M. L. Ho, H. T. Do, S. Y. Zhang, R. Kumar, D. W. Rusnak, A. K. Takle, D. M. Wilson, E. Hugger, L. Wang, F. Karreth, J. C. Lougheed, J. Lee, D. Chau, T. J. Stout, E. W. May, C. M. Rominger, M. D. Schaber, L. Luo, A. S. Lakdawala, J. L. Adams, R. G. Contractor, K. S. Smalley, M. Herlyn, M. M. Morrissey, D. A. Tuveson and P. S. Huang, *Cancer Res.*, 2006, **66**, 11100–11105.
36 C. Luo, P. Xie and R. Marmorstein, *J. Med. Chem.*, 2008, **51**, 6121–6127.
37 S. Ramurthy, S. Subramanian, M. Aikawa, P. Amiri, A. Costales, J. Dove, S. Fong, J. M. Jansen, B. Levine, S. Ma, C. M. McBride, J. Michaelian, T. Pick, D. J. Poon, S. Girish, C. M. Shafer, D. Stuart, L. Sung and P. A. Renhowe, *J. Med. Chem.*, 2008, **51**, 7049–7052.
38 J. Tsai, J. T. Lee, W. Wang, J. Zhang, H. Cho, S. Mamo, R. Bremer, S. Gillette, J. Kong, N. K. Haass, K. Sproesser, L. Li, K. S. Smalley, D. Fong, Y. L. Zhu, A. Marimuthu, H. Nguyen, B. Lam, J. Liu, I. Cheung, J. Rice, Y. Suzuki, C. Luu, C. Settachatgul, R. Shellooe, J. Cantwell, S. H. Kim, J. Schlessinger, K. Y. Zhang, B. L. West, B. Powell, G. Habets, C. Zhang, P. N. Ibrahim, P. Hirth, D. R. Artis, M. Herlyn and G. Bollag, *Proc. Natl. Acad. Sci. U. S. A.*, 2008, **105**, 3041–3046.
39 P. Xie, C. Streu, J. Qin, H. Bregman, N. Pagano, E. Meggers and R. Marmorstein, *Biochemistry*, 2009, **48**, 5187–5198.
40 G. Bollag, P. Hirth, J. Tsai, J. Z. Zhang, P. N. Ibrahim, H. N. Cho, W. Spevak, C. Zhang, Y. Zhang, G. Habets, E. Burton, B. Wong, G. Tsang, B. L. West, B. Powell, R. Shellooe, A. Marimuthu, H. Nguyen, K. Y. J. Zhang, D. R. Artis, J. Schlessinger, F. Su, B. Higgins, R. Iyer, K. D'Andrea, A. Koehler, M. Stumm, P. S. Lin, R. J. Lee, J. Grippo, I. Puzanov, K. B. Kim, A. Ribas, G. A. McArthur, J. A. Sosman, P. B. Chapman, K. T. Flaherty, X. W. Xu, K. L. Nathanson and K. Nolop, *Nature*, 2010, **467**, 596–599.
41 A. M. Alcala and K. T. Flaherty, *Clin. Cancer Res.*, 2012, **18**, 33–39.
42 A. Zambon, I. Niculescu-Duvaz, D. Niculescu-Duvaz, R. Marais and C. J. Springer, *Bioorg. Med. Chem. Lett.*, 2012, **22**, 789–792.
43 H. Yang, B. Higgins, K. Kolinsky, K. Packman, Z. Go, R. Iyer, S. Kolis, S. Zhao, R. Lee, J. F. Grippo, K. Schostack, M. E. Simcox, D. Heimbrook, G. Bollag and F. Su, *Cancer Res.*, 2010, **70**, 5518–5527.
44 K. T. Flaherty, I. Puzanov, K. B. Kim, A. Ribas, G. A. McArthur, J. A. Sosman, P. J. O'Dwyer, R. J. Lee, J. F. Grippo, K. Nolop and P. B. Chapman, *N. Engl. J. Med.*, 2010, **363**, 809–819.
45 P. B. Chapman, A. Hauschild, C. Robert, J. B. Haanen, P. Ascierto, J. Larkin, R. Dummer, C. Garbe, A. Testori, M. Maio, D. Hogg, P. Lorigan, C. Lebbe, T. Jouary, D. Schadendorf, A. Ribas, S. J. O'Day, J. A. Sosman, J. M. Kirkwood, A. M. Eggermont, B. Dreno, K. Nolop, J. Li, B. Nelson, J. Hou, R. J. Lee, K. T. Flaherty and G. A. McArthur, *N. Engl. J. Med.*, 2011, **364**, 2507–2516.
46 D. B. Solit and N. Rosen, *N. Engl. J. Med.*, 2011, **364**, 772–774.
47 R. Nazarian, H. Shi, Q. Wang, X. Kong, R. C. Koya, H. Lee, Z. Chen, M. K. Lee, N. Attar, H. Sazegar, T. Chodon, S. F. Nelson, G. McArthur, J. A. Sosman, A. Ribas and R. S. Lo, *Nature*, 2010, **468**, 973–977.
48 Q. Zhang and I. Muegge, *J. Med. Chem.*, 2006, **49**, 1536–1548.
49 A. Nicholls, G. B. McGaughey, R. P. Sheridan, A. C. Good, G. Warren, M. Mathieu, S. W. Muchmore, S. P. Brown, J. A. Grant, J. A. Haigh, N. Nevins, A. N. Jain and B. Kelley, *J. Med. Chem.*, 2010, **53**, 3862–3886.
50 X. F. Liu, H. L. Jiang and H. L. Li, *J. Chem. Inf. Model.*, 2011, **51**, 2372–2385.
51 W. Q. Lu, X. F. Liu, X. W. Cao, M. Z. Xue, K. D. Liu, Z. J. Zhao, X. Shen, H. L. Jiang, Y. F. Xu, J. Huang and H. L. Li, *J. Med. Chem.*, 2011, **54**, 3564–3574.
52 F. Bai, H. Y. Liu, L. J. Tong, W. Zhou, L. Liu, Z. J. Zhao, X. F. Liu, H. L. Jiang, X. C. Wang, H. Xie and H. L. Li, *Bioorg. Med. Chem. Lett.*, 2012, **22**, 1365–1370.
53 *Glide, version 5.5, Schrödinger*, LLC, New York, NY, 2009.
54 J. D. Hansen, J. Grina, B. Newhouse, M. Welch, G. Topalov, N. Littman, M. Callejo, S. Gloor, M. Martinson, E. Laird, B. J. Brandhuber, G. Vigers, T. Morales, R. Woessner, N. Randolph, J. Lyssikatos and A. Olivero, *Bioorg. Med. Chem. Lett.*, 2008, **18**, 4692–4695.
55 S. Wenglowsky, L. Ren, K. A. Ahrendt, E. R. Laird, I. Aliagas, B. Alicke, A. J. Buckmelter, E. F. Choo, V. Dinkel, B. N. A. Feng, S. L. Gloor, S. E. Gould, S. Gross, J. Gunzner-Toste, J. D. Hansen, G. Hatzivassiliou, B. N. Liu, K. Malesky, S. Mathieu, B. Newhouse, N. J. Raddatz, Y. Q. Ran, S. Rana, N. Randolph, T. Risom, J. Rudolph, S. Savage, L. T. Selby, M. Shrag, K. Song, H. L. Sturgis, W. C. Voegtli, Z. Y. Wen, B. S. Willis, R. D. Woessner, W. I. Wu, W. B. Young and J. Grina, *ACS Med. Chem. Lett.*, 2011, **2**, 342–347.
56 F. Zuccotto, E. Ardini, E. Casale and M. Angiolini, *J. Med. Chem.*, 2010, **53**, 2681–2694.
57 A. L. Hopkins, C. R. Groom and A. Alex, *Drug Discovery Today*, 2004, **9**, 430–431.
58 H. E. Ungnade, E. M. Roberts and L. W. Kissinger, *J. Phys. Chem.*, 1964, **68**, 3225–3228.
59 R. Morphy, *J. Med. Chem.*, 2010, **53**, 1413–1437.
60 M. S. Cohen, C. Zhang, K. M. Shokat and J. Taunton, *Science*, 2005, **308**, 1318–1321.
61 R. Kefford, H. Arkenau, M. Brown, M. Millward, J. Infante, G. Long, D. Ouellet, M. Curtis, P. Lebowitz and G. Falchook, *J. Clin. Oncol.*, 2010, **28**, 8503.
62 G. Jones, P. Willett and R. C. Glen, *J. Mol. Biol.*, 1995, **245**, 43–53.
63 G. Jones, P. Willett, R. C. Glen, A. R. Leach and R. Taylor, *J. Mol. Biol.*, 1997, **267**, 727–748.
64 M. L. Verdonk, J. C. Cole, M. J. Hartshorn, C. W. Murray and R. D. Taylor, *Proteins: Struct., Funct., Genet.*, 2003, **52**, 609–623.
65 G. M. Morris, D. S. Goodsell, R. S. Halliday, R. Huey, W. E. Hart, R. K. Belew and A. J. Olson, *J. Comput. Chem.*, 1998, **19**, 1639–1662.
66 R. Huey, G. M. Morris, A. J. Olson and D. S. Goodsell, *J. Comput. Chem.*, 2007, **28**, 1145–1152.
67 W. L. Jorgensen, D. S. Maxwell and J. TiradoRives, *J. Am. Chem. Soc.*, 1996, **118**, 11225–11236.
68 M. L. Verdonk, V. Berdini, M. J. Hartshorn, W. T. Mooij, C. W. Murray, R. D. Taylor and P. Watson, *J. Chem. Inf. Model.*, 2004, **44**, 793–806.
69 D. Fang, T. K. Nguyen, K. Leishear, R. Finko, A. N. Kulp, S. Hotz, P. A. Van Belle, X. Xu, D. E. Elder and M. Herlyn, *Cancer Res.*, 2005, **65**, 9328–9337.
70 M. Y. Hsu, D. T. Shih, F. E. Meier, P. Van Belle, J. Y. Hsu, D. E. Elder, C. A. Buck and M. Herlyn, *Am. J. Pathol.*, 1998, **153**, 1435–1442.
71 M. Fukunaga-Kalabis, G. Martinez, Z. J. Liu, J. Kalabis, P. Mrass, W. Weninger, S. M. Firth, N. Planque, B. Perbal and M. Herlyn, *J. Cell Biol.*, 2006, **175**, 563–569.
72 S. L. Johnson, D. Jung, M. Forino, Y. Chen, A. Satterthwait, D. V. Rozanov, A. Y. Strongin and M. Pellecchia, *J. Med. Chem.*, 2006, **49**, 27–30.
73 V. Pomel, J. Klicic, D. Covini, D. D. Church, J. P. Shaw, K. Roulin, F. Burgat-Charvillon, D. Valognes, M. Camps, C. Chabert, C. Gillieron, B. Francon, D. Perrin, D. Leroy, D. Gretener, A. Nichols, P. A. Vitte, S. Carboni, C. Rommel, M. K. Schwarz and T. Ruckle, *J. Med. Chem.*, 2006, **49**, 3857–3871.